Mass transfer phenomena in rotating corrugated photocatalytic reactors

Yuanyuan Xiang

Thesis submitted to the

Faculty of Graduate and Postdoctoral Studies

in partial fulfillment of the requirements for the degree of

Master of Applied Science

Under the auspices of the Chemical & Biological Engineering

University of Ottawa

Ottawa, Ontario, Canada

Sept 2013

ABSTRACT

Photocatalysis is a green technology that has been widely used in wastewater treatment. In this work, mass transfer processes in corrugated photocatalytic reactors were characterized both experimentally and through computer simulations. For the experimental work, various drum rotational speeds, reactor liquid volumes and number of corrugations were studied to elucidate their effects on mass transfer phenomena. The mass transfer rate was found to increase with increasing rotational speed. Liquid volumes in the reactor significantly affect the mass transfer rate when 20% of the surface area of the drum was immersed. A higher mass transfer rate was found using the drum with 28 corrugations, which had the lowest mass transfer coefficient when compared to the drums with 13 and 16 corrugations. In the computer simulations, velocity and concentration fields within the corrugated reactors were modelled to explore the characteristics of mass transfer processes. The mass transfer coefficients predicted by the simulations were lower than those measured experimentally due to mass transfer limitations occurring between the corrugation volume and bulk solution in the simulations. Based on mass transfer characteristics, it was determined that the drum with 28 corrugations was the most efficient photocatalytic reactor, and had the lowest mass transfer coefficient among those studied.

RÉSUMÉ

La photocatalyse est une technologie « verte » couramment utilisée pour le traitement des eaux usées. L'ouvrage ici présenté étudie, à l'aide de résultats expérimentaux et de simulations numériques, les phénomènes de transfert de matière dans des réacteurs photocatalytiques ondulés. Pour la partie expérimentale, la vitesse de rotation du réacteur, le volume d'eau dans le réacteur, et le nombre d'ondulations furent étudiés afin d'élucider leurs effets sur les phénomènes de transfert de matière. Le taux de transfert de matière augmente proportionnellement à la vitesse de rotation du réacteur. Le volume de liquide affecte significativement le taux de transfert de matière lorsque 20% de la surface du réacteur est submergée. Le taux de transfert de matière le plus élevé fut mesuré pour le réacteur à 28 ondulations, plutôt que ceux à 13 ou 16 ondulations. Lors des simulations numériques, les champs de circulation et de concentration furent caractérisés afin d'étudier le transfert de matière dans les réacteurs. Les taux de transfert de matière prédis par les simulations furent plus bas que ceux mesurés lors des expériences, dû aux limites de transfert de matière dans le liquide entre les ondulations et celui en solution qui entraient en jeux lors des simulations. L'ensemble de ces études indiquent que le réacteur à 28 ondulations, ayant le coefficient de transfert de matière le plus bas, était le plus efficace de tous ceux étudiés.

ACKNOWLEDGEMENT

I would like to express the deepest appreciation to the people who helped me during the study period in University of Ottawa.

First of all, I would like to thank my supervisor, Dr. Zhang, who gave me the opportunity to complete the Master's degree. His advice and insightful guidance through this research have been extensive and invaluable.

I am grateful to my co-supervisor, Dr. Donaldson of Dalhousie University, who introduced me to OpenFOAM software, CFD modeling, and research topics. Without his guidance and persistent help, I couldn't have finished CFD simulations.

Additionally, I would like to thank Joanne Gamage McEvoy for her kind assistance throughout my project.

Finally, I want to thank colleagues and my family for their supports and encouragements.

TABLE OF CONTENTS

LIST OF TABLES

LIST OF FIGURES

NOMENCLATURE

A	submerged surface area of benzoic acid on the corrugations (m^2)
a	the ration of submerged surface area of corrugations and water volume (m^{-1})
C	concentration of benzoic acid in water (g/L)
$C(t)$	concentration of benzoic acid at time *t* (g/L)
C_0	initial concentration of benzoic acid (g/L)
C^*	saturated concentration of benzoic acid (2.9g/L at 20°C)
c	molar concentration of mixture (mol m^{-3})
c_A	molar concentration of component A (mol m^{-3})
D_{AB}	diffusion coefficient of benzoic acid in water (1.00×10^{-9} m^2 s^{-1} at 20°C)
D_{turb}	diffusion coefficient of benzoic acid in turbulent liquid phase (m^2 s^{-1})
d	diameter of corrugated drum (m)
k_L	solid-liquid mass transfer coefficient (m s^{-1})
k_c	convective mass transfer coefficient (m s^{-1})
J_A	molar flux density of component A (mol m^{-2} s^{-1})
N_A	total molar flux of component A (mol m^{-2} s^{-1})
N_B	total molar flux of component B (mol m^{-2} s^{-1})
p	pressure (Pa)
Re	Reynolds number (dimensionless)

Re_L average Reynolds number (dimensionless)

Re_t critical Reynolds number (dimensionless)

Re_x local Reynolds number (dimensionless)

r radius of corrugated drum (m)

S_ϕ source term in governing equation

Sc Schmidt number (dimensionless)

Sc_{turb} turbulent Schmidt number (dimensionless)

Sh Sherwood number (dimensionless)

Sh_L average Sherwood number (dimensionless)

Sh_x local Sherwood number (dimensionless)

t experimental time (min)

t_0 initial experimental time (min)

U velocity (m s^{-1})

u velocity (m s^{-1})

V volume of solution in reservoir (m^3)

y_A molar fraction of component A (dimensionless)

z position (m)

Greek symbols

α dimensionless concentration of benzoic acid (dimensionless)

Γ_ϕ diffusion coefficient in governing equation

υ kinematic viscosity ($m^2\ s^{-1}$)

υ_{turb} turbulent kinematic viscosity ($m^2\ s^{-1}$)

ρ density ($kg\ m^{-3}$)

ω angular velocity of rotating drum ($rad\ s^{-1}$)

ϕ general variable in governing equation

CHAPTER 1

Introduction

1.1 Background

With the increase of environmental pollution and destruction, new environmental-friendly technologies and clean chemical processes are urgently needed. Photocatalysis is a one such technology which can operate at room temperature under irradiation to convert many harmful environmental pollutants into benign products such as CO_2 and water, and has been studied for a variety of applications ranging from anti-fogging, anti-bacterial and self-cleaning surfaces, to water and air purification.

Photocatalysis used for wastewater treatment has been rapidly developed in recent years and the efficiency of photocatalytic reactors remains the most important issue in photocatalytic systems design. In order to optimize the efficiency realized in photocatalysis, several novel reactor designs have been proposed and investigated in the literature, such as annular photoreactors, rotating disc photoreactors and corrugated photoreactors. Many researchers have found that mass transfer limitations which occur in photocatalytic reactors significantly influence the decomposition of pollutants, and the resulting photocatalytic efficiencies obtained. Thus, it is necessary to analyze the mass transfer phenomena in photocatalytic

reactors for the improvement of contaminant degradation and future optimization of photocatalytic processes.

1.2 Objective

The main objectives of this research are the experimental and computational analysis of the mass transfer processes in corrugated photocatalytic reactors prepared with different corrugation angles. This research was performed on a novel corrugated photocatalytic reactor previously developed in our group.

1.3 Thesis outline

This thesis consists of three parts. The first part, Chapter 2, presents a literature review of mass transfer studies in various photocatalytic reactors. It includes discussion of: the mechanism of mass transfer, methods to measure the mass transfer coefficient, effects of mass transfer on photocatalysis processes, and mass transfer limitations within photocatalytic reactors. The second part, Chapter 3, discusses experimental and computational results of mass transfer in corrugated photoreactors with various degrees of corrugation. The effect of drum rotational speed, reactor liquid volume, and number of corrugations on mass transfer phenomena were investigated experimentally. The velocity and concentration patterns within reactors were simulated by computational fluid dynamics (CFD) and mass transfer coefficients obtained by simulation were compared with the experimental values. Finally, conclusions and future work are discussed in Chapter 4.

CHAPTER 2

Mass transfer aspects to photocatalytic waste treatment: A Review

Abstract

Photocatalysis has received a great deal of attention in the last three decades for its potential as an efficient solution to a number of environment problems. It is a green technique that is capable of degrading otherwise recalcitrant pollutants into water and carbon dioxide under irradiation. Mass transfer processes in photocatalytic reactions significantly influence the degradation rates of contaminants. In this article, an introduction of the principles of photocatalysis and mass transfer is given and extended to the review of mass transfer aspects of photocatalytic processes. Experimental measurement techniques and computational fluid dynamic simulations of mass transfer coefficients are discussed with respect to efforts made by researchers in recent years. Understanding the effect of factors on mass transfer and mass transfer limitations encountered in different photocatalytic reactors is essential for the development of improved reactor designs, facilitating their operation, and enabling the optimization of photocatalytic processes.

2.1 Introduction

With the rapid growth of population and economic development, the demand for clean water

increases each year. In addition to the unsustainable utilization of water for industry and agriculture, as well as long-term droughts, the shortage of clean water resources has become an important issue worldwide. It is estimated that around four billion people worldwide lack access to clean and sanitized water, and millions of people die of waterborne diseases each year [1]. To address these issues and attempt to reduce water scarcity problems, development and utilization of unavailable water resources, for example through sea water desalination, can present a viable approach. However, these strategies cannot represent a main method of providing clean water due to the high-cost and low efficiencies realized with these advanced technologies. Additionally, the amount of wastewater discharged from households and manufacturing plants is also a major contributor to global water pollution and shortage issues [2]. In order to alleviate the clean water crisis, wastewater treatment technologies aimed at facilitating water reuse and recycling are desirable.

Wastewater treatment encompasses all processes used to treat waters that contain bacteria, chemicals, and other contaminants from industrial activities, to make them suitable for discharge into the environment or for reuse. To meet the necessary safety criteria, the contaminants in the wastewater must be reduced to an acceptably low level prior to release into the environment. The wastewater treatment technologies may be classified into four major categories: biochemical, physical, chemical, and physicochemical methods, respectively [3]. Biological treatment technologies use bacteria and other biological matter to break down waste. However, these methods are generally low efficiency and could cause

secondary pollution to the environment. Physical wastewater treatment begins with removing suspended solids from wastewater. An example is adsorption or coagulation, which are processes that concentrate the pollutants by transferring them into other phases, however, this does not lead to their ultimate destruction [4]. Other conventional water treatment methods such as chemical, membrane technologies or ion exchange methods, especially intensive chemical treatments involving ammonia, chlorine compounds, and hydrochloric acid, could generate toxic secondary pollutants into the ecosystem, aggravating the water problems and influencing human health [1].

Advanced Oxidation Processes (AOPs) are innovative water treatment technologies that can be used for decontamination of water containing organic pollutants. AOPs rely on *in-situ* generation of highly reactive species ($\cdot OH$, O_2^-) which are strong oxidants that can virtually oxidize any compound present in the water [5]. Among the AOP technologies, heterogeneous photocatalysis, based on the use of wide-band gap semiconductor catalysts (TiO_2, Fe_2O_3, and ZnO) in conjunction with irradiation by UV light, has become an attractive method for wastewater treatment. Photocatalysis possesses significant advantages over the traditional methods and other AOPs in water treatment [6]. Specifically, photocatalysis is able to degrade and mineralize the organic compounds completely to carbon dioxide and water. TiO_2 is readily used as a photocatalyst because it is inexpensive, non-toxic, chemically stable and highly photocatalytically active [7]. The light required to activate the catalyst is low-energy UVA for photo excitation, and it is also possible to use solar light as an alternative. Therefore,

TiO_2-mediated photocatalysis represents a clean technology in which little polluted substance remains after treatment.

The purpose of this review is to give an overview of current understanding and investigations of mass transfer processes in photocatalytic applications through discussions of the mechanism of photocatalysis and mass transfer, measurements of mass transfer coefficients, computational fluid dynamic simulations on mass transfer, the influence of various factors on mass transfer, and mass transfer limitation studies in photocatalytic reactors.

2.2 Fundamental of photocatalysis

Semiconductor photocatalysis is initiated by the pairs of electrons and holes generated by the photocatalyst upon band gap excitation [8]. When a photocatalyst absorbs ultraviolet radiation (either from sunlight or artificially produced by a lamp), it will produce pairs of electrons and holes. If the energy obtained from light is greater than the band-gap energy of the photocatalyst, the excited electrons from valence band will jump to the conduction band, creating negatively charged electrons and leaving behind positive holes in the valence band.

$$Photocatalyst \overset{hv}{\rightarrow} {e_{cb}}^{-} + {h_{vb}}^{+} \quad (1)$$

The free electrons and the positive holes are highly charged and can be used in number of reduction and oxidation reactions. For example, the positive holes are able to break apart water molecules to form hydrogen gas and hydroxyl radicals, and the negative electrons may react with oxygen to form oxide anions [9]. These radicals can ultimately be used to

decompose the water contaminants. For heterogeneous photocatalysis, liquid phase organic compounds are degraded to their corresponding intermediates and further mineralized to CO_2 and water after prolonged irradiation.

The overall photocatalysis reaction can be divided into five independent steps [10]: (1) organic contaminant is transported from the liquid phase to the catalyst surface; (2) contaminant is adsorbed onto the surface, which has been activated by photon energy; (3) the adsorbed liquid phase undergoes surface reaction; (4) produced reaction intermediates are desorbed from the catalyst surface; and (5) intermediates are transported from the interface of liquid and solid to the bulk fluid. The first and last steps are mass transfer processes, while the others are chemical reactions. The overall rate of photocatalytic reaction is determined by the slowest step in these five sequential processes. If the mass transfer occurs faster than the involved reaction steps, the concentrations of contaminant are identical in the active region and the bulk liquid phase. To ensure the efficiency of photocatalytic reactions, and to prevent the mass transfer limitations on the overall photocatalytic rate, the mass transfer processes involved must be well characterized, and subsequently maximized. Therefore, greater understanding these mass transfer processes in photocatalytic reaction and reactors is a significant issue.

2.3 Mass transfer mechanism

Mass transfer is a net movement of matter from one place to another due to the difference

concentration between locations. It is a natural tendency for mass to be transferred from areas of high chemical potential to areas of low chemical potential, minimizing any difference within the system. Generally, chemical species transfer between two phases through an interface or by diffusion through one phase. These phenomena are often illustrated by common examples, such as the dissolution of sugar into water, diffusion of cigarette fumes into air, or the use of chemical dyes to pigment textiles. Mass transfer is also prevalent in many chemical engineering processes, such as evaporation, absorption and desorption in gas-liquid systems, extraction in liquid-liquid systems, and crystallization in liquid-solid systems [11]. The study of mass transfer phenomena is significant for the design of mass transfer systems, such as plate and distillation columns, as well in the design of as chemical reactors in order to understand the influence of mass transfer on chemical reactions. In recent years, ongoing research has been conducted on the study of mechanisms and effect of transport phenomena in various operations in order to optimize various industrial processes [12-15].

Generally, there are two main routes for the transport of species within a physical system, namely, molecular mass transfer and convective mass transfer. The former one results from the thermal motion of all particles in the presence of any concentration gradient or other forces, while the latter results from the large-scale motion of currents in the fluids.

2.3.1 Molecular mass transfer

The transfer of mass by diffusion was first described by Brown in 1827 [16]. At a molecular level, every molecule follows a random path due to interaction with other molecules and tends to fill volume available to it [17]. For example, consider two different gases which occupy two separate rooms, but are connected by a tube. If these two gases are maintained at the same temperature and pressure, but are at different concentrations, then each gas will run through the tube into the other room to maintain a uniform concentration in the system. Despite the fact that the concentration of each gas is at equilibrium, the gases still diffuse but the net fluxes are zero. The system described is said to be under dynamic balance. Such mass diffusion processes occur not only in gases, but also in liquid and solid phases.

The rate of molecular diffusion is described mathematically by Fick's first law, which given by equation (2)

$$J_A = -cD_{AB}\frac{dy_A}{dz} \tag{2}$$

where J_A is the molar flux density of component A (mol/m^{2}s), c is molar concentration of mixture (mol/m^3), D_{AB} is the diffusion coefficient of component A into component B (m^{2}s), and $\frac{dy_A}{dz}$ is concentration gradient in the direction that diffusion occurs. Fick's first law can be only applied for the diffusion caused by random motion of molecules. If the diffusion occurs with bulk flow, the molar flux resulting from the bulk flow should be considered in conjunction with Fick's first law to calculate the total molar flux. The expression to describe this case is given by:

$$N_A = -D_{AB}\frac{dc_A}{dz} + y_A(N_A + N_B) \tag{3}$$

where y_A is the molar fraction of component A. N_A and N_B are the total molar fluxes of component A and B (mol/m^2s), respectively.

2.3.2 Convective mass transfer

Convective mass transfer is the transport process that occurs between a solid surface and a moving fluid or in two immiscible moving fluids. There are two types of convective mass transfer: a pump, rotor, or a similar device causing motion resulting in mass transfer is classified as forced convection, while mass transport due to density differences classified as free or natural convection.

2.3.2.1 Mass transfer at a boundary layer

Understanding the mechanism of convective mass transfer is very important in the study of mass transfer processes. As the fluid flows over a surface under turbulent condition, the turbulent boundary layer occurs after sufficient development. It consists of three parts: a laminar sub-layer which is near the surface, a buffer layer near the laminar layer, and an outermost turbulent part which occupies the majority of the boundary layer [11](Figure 2.1). The mass transfer mechanisms which occur in these three layers are extremely different. In the laminar layer, fluid flows parallel along the surface. There is only random molecular motion occurring in the direction perpendicular to fluid flow. Thus, the mass transfer that occurs between the surface and fluid is based on molecular diffusion, which can be described by Fick's first law. In the buffer layer, eddy motion appears within the laminar flow. The

mass transfer includes the molecular diffusion which is close to laminar sub-layer, as well as eddy diffusion which is near the turbulent flow layer. In the turbulent flow layer, a number of eddies exist and vigorously flow. In this section of the boundary layer, eddy mass transfer is the main manner of mass transport and the effect of molecular diffusion can be neglected. Since the fluid is intensively mixed in the turbulent zone, the concentration gradients in this area are relatively low. However, the concentration gradients present in the laminar sub-layer are much greater due to the lack of these eddies.

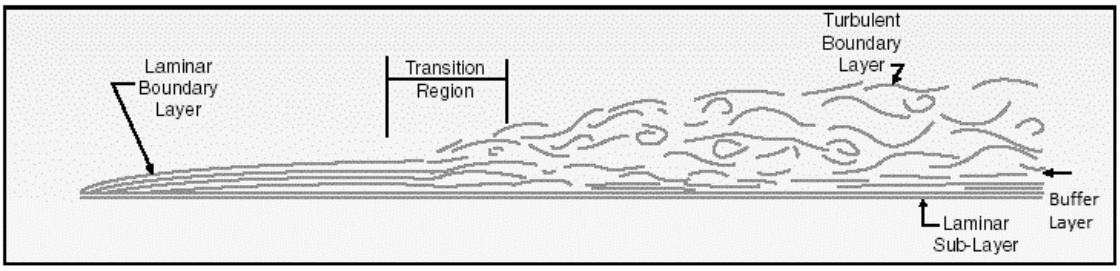

Figure 2.1 Turbulent boundary layer [18]

2.3.2.2 Mass transfer coefficient

The rate of convective mass transfer is not only a function of characteristic factors of mass transfer but is also related to the dynamic factors of momentum transfer. The basic equation of convective mass transfer is described below:

$$N_A = k_c \Delta c_A \tag{4}$$

where N_A is the molar flux of convective mass transfer(mol/ m^2s), k_c is the convective mass transfer coefficient(m/s) and Δc_A is the difference between the concentration of component A at the interface and in the bulk of the fluid (mol/ m^3). The definition of k_c here is based on the

concentration difference. Since the concentration can be expressed as many other units, such as pressure, density and molar fraction, the convective mass transfer equation can adopt many forms. Generally, mass transfer coefficient is a function of flow pattern, concentration gradient, geometry of the interface, and fluid properties, etc. It is a key factor in the calculation the mass transfer rate. The methods used to describe these mass transfer coefficients vary according to the mass transfer process, and are further detailed in subsequent sections.

2.3.3 Dimensional analysis of mass transfer

To study mass transport processes, dimensional analysis is commonly used. The application of this analysis to the description of mass transfer yields three nondimensional groups, namely: the Reynolds, Sherwood, and Schmidt numbers, respectively. These numbers relate the mass transfer coefficient k with the equivalent diameter d, the kinematic viscosity of the fluid ν, and the diffusivity D_{AB} according to the following relationships:

$$Re = \frac{ud}{\nu} \tag{5}$$

$$Sh = \frac{k_l d}{D_{AB}} \tag{6}$$

$$Sc = \frac{\nu}{D_{AB}} \tag{7}$$

Researchers have found correlations of these nondimensional values to yield empirical solutions for the mass balance of the system. For most cases, the correlation is of the form:

$$Sh = aRe^b Sc^c \tag{8}$$

The values of parameters, a, b, c, can be obtained by experiments or calculated from differential equations.

A numbers of correlations have been published for both specific and representative systems. For example, the correlations for fluid flow on one side of a flat plate are of the form:

$$Sh_x = 0.332 Re_x^{0.5} Sc^{0.33} \qquad for\ Re_x < 2 \times 10^5 \tag{9}$$

$$Sh_L = 0.664 Re_L^{0.5} Sc^{0.33} \tag{10}$$

$$Sh_x = 0.0292 Re_x^{0.8} Sc^{0.33} \qquad for\ Re > 2 \times 10^5, Re_t = 2 \times 10^5 \tag{11}$$

$$Sh_L = 0.664 Re_t^{0.5} Sc^{0.33} + 0.0365 Sc^{0.33} [Re_L^{0.8} - Re_t^{0.8}] \tag{12}$$

for laminar and turbulent conditions, respectively [19].

Such mass transfer correlations are useful for reactor design optimization, as well as for analysis of chemical kinetics. The development of these mass transfer correlations is crucial in the understanding of mass transfer processes. In light of this, it should be considered that mass transfer processes are similar with heat and momentum transport phenomena in that if a complex case cannot be solved by analysis of the mass transfer problem only, a mathematical model used for heat or momentum transfer can be transferred to solve mass transfer problem by using analogy between them.

2.4 Mass transfer measurement

Most engineering problems involving mass transfer have convective phenomena caused by fluid flow either under laminar or turbulent conditions. Since the mass transfer coefficient is

one of the most important parameters for design and operation of chemical reactors, a variety of methods have been used to measure these coefficients experimentally.

2.4.1 Dissolution method

The dissolution method measures an average mass transfer coefficient using integral measurements of different concentrations of dissolved material obtained at various time points. It is a widely used method for measuring solid-liquid mass transfer coefficients based on the liquid saturation limit of the dissolved solid. The solid material can be benzoic acid [20-23], β-naphthol [24], potassium permanganate, potassium sulfate. The solubility of the solid must remain low in order to avoid variation of the interfacial area of solid and liquid. In these experiments, water is often used as liquid phase.

Hixon and Baum analyzed the mass transfer coefficients in liquid-solid agitated systems using a number of solutions such as: benzoic acid in water, cotton seed oil, benzene, methanol, glycol, and sucrose solutions, naphthalene in methanol, barium chloride in water, and rock salt in water [25]. Abdel-Aziz et al. studied the rate of liquid-solid mass transfer controlled processed in helical tubes by dissolving the copper tubes in acidified dichromate [26]. Pitault et al. measured the local liquid-solid mass transfer coefficients of two types of three-phase laboratory scale reactors equipped with stationary catalytic basket and multiple impellers by using naphthol particle dissolution in n-heptane at several agitation speeds [27]. Another solid-liquid mass transfer coefficient was investigated using salicylic acid loaded

onto silica gel particles, dissolved in water to study the hydrogenation of 4-nitrobenzaic acid in a stirred reactor [28].

Dissolution is the simplest and easiest method for measuring mass transfer coefficient, and introduces little error at atmospheric conditions. This method uses the assumption that the liquid is well mixed, and usually allows for the average mass transfer coefficient to be obtained. The solid materials used can be coated on the reactor surface by dipping, brushing, or spraying. However, for some reactors involving complex assembly or many parts, a substantial amount of the coating may dissolve in the liquid when placed into the reactor before the experiment has even started [29]. Moreover, noticeable losses in the dissolved material can be observed as a result of flashing or stripping from the liquid phase to the atmosphere and the effluent gas stream in studies involving low pressures in two-phase flow packed–bed reactors [30]. These difficulties lead to deviations in the measured coefficients, which could result in misunderstanding the effect of reactor pressure and improper conclusions drawn from the study.

2.4.2 Naphthalene sublimation method

The naphthalene sublimation technique is generally employed to determine the solution to a heat transfer problem by means of an analogous mass transfer problem. It often used to investigate the mass transfer rate at an air-solid interface, because naphthalene sublimes at room temperature. The low toxicity, and good casting and machining properties of

naphthalene have also promoted the rapid development of this technique [31]. The steps involved in the naphthalene sublimation method are as follows. The test specimens are first coated with naphthalene, and the initial naphthalene surface profile or weight are measured. The surface profile or weight are then measured again after the experimental operation, and the data is analyzed by difference to obtain the mass transfer coefficient [32].

The naphthalene sublimation method has been applied to various studies. For example, an experimental study on mass transfer from a circular cylinder in pulsating free stream was conducted by employing this technique [33]. The naphthalene sublimation method was also used to investigate the surface flow pattern and local mass transfer characteristics on the free end surface of a finite circular cylinder [34], and to study the mass transfer on a flat plate [35]. Kwon et al. used this method to investigate the local and average heat/mass transfer characteristics on a single dimple [36], while Yoo et al. obtained the local heat/mass transfer coefficient for two flow conditions and investigated the effect of boundary layer [37]. Then they investigated how separated and reattached flow affects mass transfer by comparing the transport characteristics on an inclined flat plate with those on a parallel flat plate [38].

A mass transfer test using the naphthalene sublimation technique is easily performed experimentally and facilitates ease of handling. The casting naphthalene-coated specimen is the only one needed, and the local mass transfer rates are obtained by measurements of the sublimation depths. The most important advantage of this method is that it can be converted to heat transfer results by a mass transfer analogy. The isothermal and adiabatic boundary

conditions in heat transfer measurements can be imposed with little error in mass transfer experiments by using a surface coated with naphthalene as an isothermal and nonsubliming surface in analogy with an adiabatic boundary condition [32]. Thus, the convective component of heat transfer can be estimated in mass transfer experiments, and the conduction and radiation errors are eliminated. However, once the uniform layer of naphthalene has been completely removed at any location, the mass transfer analogy for uniform surface concentration is consequently lost, leading to significant errors [39].

2.4.3 Electrochemical method

The electrochemical method or limiting current method represents a process for the evaluation of mass transfer rates between a liquid and an electrode. This technique has been widely used in studies of liquid-solid mass transfer coefficients for a rough surface in complex flow regimes or for chemical reaction systems. It is based on the measurement of the maximum achievable current through an electrode for a particular electrochemical process [40]. The electric current is a function of the potential applied between the cathode and the anode and it increases exponentially with increasing potential until it approaches a constant value which is called the limiting current. The mass transfer coefficient can be expressed as

$$k = \frac{I_{lim}}{nAFC_B} \tag{15}$$

where I_{lim} is the limiting current, n is the number of exchanged electrons, A is the electrode

surface area, F is the Faraday constant and C_B is the bulk concentration in solution.

The limiting current technique can be used for electrochemical reactors to analyze the effect of electrode configuration on mass transfer rates [41, 42]. It was applied to measure the liquid mass transfer coefficient in an empty pipe by Xu et al., and the authors indicated that this method was excellent in measuring coefficient of both single phase flow system and multiphase flow system [43]. The materials of electrode and liquid vary from study to study. The process of cathodic copper deposition for the measurement of limiting current was chosen for the assessment of mass transfer performance at a spinning disc reactor system [40]. A cupric acid–copper sulfate electroplating system was also adopted to investigate the effects of the anode size and position on the limiting currents of natural convection mass transfer experiments in a vertical pipe [44]. Another electrolytic cell, ferri-ferrocyanide system and nickel electrodes, was used to obtain the mass transfer coefficients in an annular duct with an obstruction [45]. Additionally, Abdel-Aziz studied the mass transfer rate at a horizontal cylinder placed in a cylindrical vertical column under different hydrodynamic conditions by measuring the limiting current of the cathodic reduction of $K_3Fe(CN)_6$ using a solution containing $K_3Fe(CN)_6$ and $K_4Fe(CN)_6$ and excess NaOH as supporting electrolyte [46].

The limiting current technique is relatively simple, fast, and inexpensive. The accuracy of measuring the mass transfer coefficient is better that obtained using other techniques such as dissolution method. The most important advantages of electrochemical methods are that the

driving forces can be easily controlled and the current, which corresponds to the transport rate, can be readily and precisely monitored in situ [47]. However, the reduction of liquid conductibility resulting from degradation of the electrolyte can lead to variation in local mass transfer coefficients. Moreover, the electrolyte has a limited useful lifetime and film formation on the electrode surface after longer operation times was previously reported [48]. The composition of the film in the ferri-ferrocyanide system indicated that ferri-/ferrocyanide decomposition products were precipitating onto the surface and this reduced the limiting current since it rendered a portion of the active surface inert.

2.4.4 Absorption method

The absorption method is often used for gas-liquid mass transfer. An overall mass transfer coefficient is adopted to analyze the transport processes, and consists of a liquid-side mass transfer coefficient and a gas-side mass transfer coefficient with a partition constant. For a highly soluble gas, the gas phase dominates the mass transfer process with no liquid-side resistance. The overall mass transfer can be expressed as using a gas mass transfer coefficient. However, in the case where the liquid phase dominates the mass transfer, liquid mass transfer coefficient may be applied for a sparingly soluble gas condition.

For the liquid-side mass transfer rate, a physical absorption of sparingly soluble gases, typically oxygen or carbon dioxide, in water is generally used to measure the mass transfer coefficients [49]. As oxygen or carbon dioxide has a low solubility in water, there is no

significant gas-side resistance. The driving force in the gas can be determined either by the concentration or pressure. Yue et al. used pure carbon dioxide in the physical absorption method and the amount of absorbed CO_2 in water was determined by adding the liquid sample into an excess of NaOH solution and titrating with HCl solution [50]. Similarly, Fan et al. measured the pressure of N_2 above the liquid methanol interface after gas was exposed to the liquid in a milliliter-scale slurry reactor system [51].

Chemical absorption is often selected instead of physical absorption to measure the gas-side mass transfer rate. The use of reactive absorption enables the separate determination of mass transfer coefficients and the interfacial area [52]. The absorption of SO_2 in aqueous NaOH solutions is an example of this kind of system, which can be used together with the CO_2 absorption in aqueous NaOH to determine the gas-side mass transfer coefficients [53]. The absorption of oxygen in sulfite solutions is another widely used method for determination of mass transfer characteristics [54]. In this chemical system, oxygen reacts with a solution of sodium sulfite and can be catalyzed by metal ions. Additionally, chemical absorption can be employed for the measurement of liquid- side mass transfer coefficient. The absorption of CO_2 into a buffer solution of $NaHCO_3/Na_2CO_3$ is generally chosen. Since the first-order rate constant for this chemical absorption reaction is close to the constant for the physical absorption, the reaction rate should be much slower than the mass transfer rate of CO_2 into the solution, thus the chemical absorption process can be treated as a physical one [50].

The absorption method enables the measurement of the liquid or gas-side mass transfer

coefficients by the careful selection of appropriate gas solubility in the liquid phase. However, for the chemical absorption method, the high absorption rate due to chemical reaction could cause the bubble to shrink, decreasing the interfacial area observed [55]. This variation of interfacial area should be considered to evaluate the mass transfer coefficient values. Also the concentration of the liquid phase which influences the reaction rate should be controlled to reduce the experimental error.

2.5 CFD modeling

Computational fluid dynamics has become an indispensable tool for engineering problems. CFD simulations provide insight into the details of how processes work and allow the evaluation and optimization of the simulated system by a computational solution, even before prototypes have been built. The features of simulation, such as low cost, short lead times, and satisfactory accuracy, enable CFD to be a convenient and useful method to study many engineering processes [56].

In order to simulate the mass transfer processes in chemical engineering, the flow pattern should be first investigated. The fluid is described as a continuum and the governing equations of fluid dynamics, the mass, momentum and energy equations provide the cornerstone of CFD. These equations have significant commonalities so that a general variable ϕ can be used to describe the conservative form of all fluid flow equations, including equations for scalar quantities such as temperature and concentration. This common

governing equation is written in the following form:

$$\frac{\partial(\rho\phi)}{\partial t} + \nabla \cdot (\rho U\phi) = \nabla \cdot \left(\Gamma_\phi \nabla\phi\right) + S_\phi \qquad (16)$$

where the variable ϕ can be velocity along x, y, and z direction, temperature or mass fraction, ρ is the density of fluid, Γ_ϕ is the diffusion coefficient, and S_ϕ is the source term.

Turbulent flow is the most common condition that is simulated in CFD. It causes the formation of eddies with a wide range of length and time scales that interact in a dynamically complex way. The numerical methods to capture the turbulent characteristics can be grouped into the following categories, as discussed in subsequent sections.

2.5.1 Turbulent flow

2.5.1.1 Direct numerical simulation (DNS)

Direct numerical simulation (DNS) is the most natural and straightforward approach in that these simulations directly compute the mean flow and all turbulent velocity fluctuations. In this approach, the Navier-Stokes equations are solved on sufficiently fine mesh which can resolve the Kolmogorov length scales and with time steps sufficiently small to resolve the period of the fastest fluctuations.

Since DNS is costly in term of computing resources, it is only useful for flows with low Reynolds numbers. The applications of DNS are therefore limited to turbulence research and results from DNS simulations can be important to verify results from other turbulence models.

2.5.1.2 Large eddy simulation(LES)

Large eddy simulation (LES) tracks the behavior of the large eddies due to the fact that the large scale motions are generally more energetic than the small scale ones. The method involves low-pass filtering which eliminates the small scales of the solution [57], reducing the computational cost of the simulation. LES is preferred over DNS when the Reynolds number is high or the computational domain is complicated.

2.5.1.3 Reynolds-averaged Navier-Stokes equations(RANS)

Generally, the DNS and LES approaches give very detailed information about the flow, so they require high usage of computational resources. For most engineering purposes, it is unnecessary to resolve the details of turbulent fluctuations. Reynolds-Averaged Navier-Stokes models can be chosen in these cases to suit the needs of the research. The RANS models focus on the mean flow and the effects of turbulence on mean flow properties. Navier-Stokes equations are time averaged and the extra terms which are caused by the interactions between various turbulent fluctuations appear in the time-averaged flow equations [56]. These extra terms can be modeled with various types of RANS models, such as the standard k-ε model, realizable k-ε model, k-ω model, and the Reynolds stress model etc, depending on the flow conditions and computational domain [58]. These models are further discussed below.

2.5.1.3.1 The standard k-ε model

The standard k-ε model is the most widely used and validated model due to the important role played by ε, which is the energy-dissipation rate, which appears directly in the transport equation for k, the turbulent kinetic energy. This model is suitable for high Reynolds numbers, and provides a good compromise between generality and economy for many CFD problems. However, it is not good for round jets and flows involving significant curvature, swirl, and separation [56].

2.5.1.3.2 The realizable k-ε model

The difference between this model and standard k-ε model is that a realizability constraint on the predicted stress tensor is considered in this model, and it involves a modification of the ε equation. This modification of standard k-ε model gives improved simulation for swirling flows and flow separation. Despite this, it is not as stable as the standard k-ε model.

2.5.1.3.3 The k-ω model

In this turbulence model the specific dissipation, ω, is used as the length-determining quantity, defined by $\omega \propto \varepsilon/k$. This model is advantageous compared with the k-ε model due to its superior performance in regions with low Reynolds number and its availability with adverse pressure gradients and separating flows. However, this method requires very fine mesh close to the wall.

2.5.1.3.4 Menter SST k-ω model

Since the results of k-ε model are less sensitive to the assumed values in the free stream and

its near-wall performance is unsatisfactory for boundary layers with adverse pressure gradients, SST k-ω model uses a transformation of the k-ε model into a k-ω model in the near-wall region and the standard k-ε model in the fully turbulent region far from the wall [59]. This model is recommended to replace the k-ε model as a choice [56]. It works well with adverse pressure gradients and separating flow, but it over-predicts turbulence in regions with large normal strain.

2.5.1.3.5 Reynolds stress model

This model abandons the isotropic eddy-viscosity concept, which is the primary weakness of the previous models, and solves the transport equations for Reynolds stress and the energy-dissipation rate, ε. It accounts for anisotropy and is applicable for complex flow. However, the computation of this type of model is expensive due to the numbers of equations solved.

2.5.2 Turbulent flow and mass transfer modeling studies

In turbulent flow regimes, the molecules of a substance are transported from one place to another along the flow. To model the mass transfer processes taking place, the mass fraction of a particular component can be modeled by CFD based on the velocity and pressure obtained from turbulent flow of fluid, and CFD simulations have been applied to mass transfer studies in many publications.

The RANS approach of turbulent flow modeling has been the mainstay of flow calculations over the last three decades. Moraveji et al. investigated the hydrodynamics and mass transfer

for two phase bubbly flow in a split cylindrical airlift reactor using experimental data and CFD simulations [60]. The k-ε model was chosen to simulate the turbulent flow. Zambra et al. studied a tridimensional mathematical model that considered the turbulent flow inside a bioreactor of municipal waste material, where the turbulence was also treated by the k-ε model [61]. Zhang et al. investigated the effect of photocatalytic surface roughness on reactors' effectiveness for indoor air purification using a realizable k-ε model to simulate the air flow properties in a model photoreactor channel [62].

The differences between various RANS models are also investigated. Esteban Duran et al. modeled the mass transfer process in an annular reactor which can be used as an immobilized photocatalytic reactor [63]. Different hydrodynamic models were evaluated against experimental data in terms of mass transfer prediction capabilities, including laminar, standard k-ε, realizable k-ε, Reynolds stress(RSM), and the Abe-Kondoh-Nagano(AKN) models. It was found that the laminar model successfully predicted the mass transfer in laminar flows, while the AKN and the RSM models performed well and the relative error of the estimations of the entire reactor were approximately 10% and 20%, respectively. Moreover, the AKN model provided a better prediction of average mass transfer rates among the four models and the RSM also operated well, except that it predicted lower mass transfer rates at the entrance region.

Mass transfer models are often chosen for waste treatment applications. Global and local mass transfer coefficients in waste water treatment processes were measured by the CFD

code ASTRID in two-phase flow reactors to optimize the design and control on the operation [64].

The effect of airflow and aqueous ammonium solution temperature on ammonia mass transfer from an emitting surface was studied, where the surface concentration distribution and mass transfer coefficients at different temperatures and velocities were investigated using a CFD model [65].

Oxygen transfer in a high-speed surface aeration tank for wastewater treatment was simulated by a CFD model, and was validated through a full-scale aeration test [66].

Another transient CFD modeling of toluene waste gas biodegradation in a three-phase airlift loop reactor was performed [67]. This 3D transient CFD model developed for the simulation included the k-ε model, interphase forces, momentum and mass transfer, bubble coalescence and breakup, and the bioreaction.

Similarly, a mathematical model using CFD techniques was used to study the mass transfer and shear in an airlift bioreactor [68]. The model analyzed an existing geometry of an airlift bioreactor and validated the modification on the initial design. The new design showed an increase in the mass transfer along with a decrease of shear stress.

Applications of CFD are widely developed for not only pure mass transfer phenomena, but are also coupled with other processes such as chemical reactions or heat transfer. CFD simulation has become a reliable tool to assist in understanding fluid flow process and the design of reactors.

2.6 Effects on mass transfer

In transport processes, the rate of mass transfer in a reactor is determined by the mass transfer coefficient, the interphase interfacial area, and the driving force in concentration. The mass transfer coefficient can be determined by the diffusion of the solute, or by the surface renewal rate of the fluid near the interface. Generally, surface renewal rate can be increased by agitating the fluid or flowing the liquid with a high velocity through the reactor. The effect of fluid flow parameters on mass transfer has therefore been studied in-depth by various researchers in order to better understand and to increase the observed mass transfer rate.

2.6.1 Effect of fluid velocity

Since the fluid flow influences the convective mass transfer, many researchers have studied the effect of the flow rates in various reactors.

Koide et al. investigated the effects of gas velocity, column dimensions and properties of the liquid and solid particles on volumetric mass transfer coefficient in a three-phase internal loop airlift reactor [69]. Muthukumar et al. also studied the influence of organic additives on the volumetric mass transfer coefficient in an internal loop airlift reactor [70]. In both of these studies, it was reported that the mass transfer coefficient increased with increase in gas velocity and decreased with increase in solids loading.

Chen et al. studied the effect of mass transfer and catalyst layer thickness in photocatalytic

reactions and found that both external and internal mass transfer played significant role in photocatalytic processes [71]. The experimental data obtained also confirmed the result that mass transfer coefficient increased with increasing circulating flow rate.

2.6.2 Effect of rotational speed

Rotating disc or cylinder reactors have been used for several applications including dissolution of solids into solvents and in the preparation of catalysts. The application of these reactors for semiconductor photocatalysis has attracted a considerable amount of research interest in the field of wastewater treatment [72]. The rotational speed had been reported to be the dominant factor influencing the mass transfer processes involved, and the effect of this parameter has been studied by many researchers.

For example, Dionysiou et al. studied the oxidation of organic contaminants in a rotating disk photocatalytic reactor and analyzed the role of mass transfer in the chemical reaction process [73]. The results for the overall mass transfer coefficient for 4-CBA at different disk angular velocities suggested that the mass transfer coefficient increased with increasing of rotating speed.

Hamill et al. used a batch rotating photocatalytic contactor for the degradation of organic pollutants in wastewater [74]. In this study, the bulk solution transitioned from the laminar flow regime into a turbulent one with increased rotational speeds, and much improved mixing and transport to the catalyst surface was observed. The relation of overall mass

transfer coefficient for the VOC air stripping and rotational speeds presented a sharp break in the gradient at 90 rpm corresponding to the transition point between the penetration and film theories. In the penetration theory, poor transport perpendicular to the disc surface exists in the entrained film on the discs, while in film theory, eddies and turbulent mixing occur within the liquid film ensuring good mixing and transport to the disc surface. Therefore, the mass transfer coefficients are only a function of disc rotation speed.

2.6.3 Effect of agitation speed

Mixing and agitation of a fluid affects the number and flow of eddies which may appear, significantly promoting the molecule motion and mass transfer.

Leon et al. studied hydrodynamics and gas-liquid mass transfer in a horizontal rotating foam stirrer reactor [75]. From this study, the gas-liquid mass transfer rate increased almost linearly with the stir speed in a partially filled horizontal reactor. The increase of mass transfer with the stir speed is due to a combination of increased amount of bubbles created by the turbulence at gas-liquid interface and higher relative velocity between bubbles and liquid. At a higher rotational speed, the large bubbles break up into smaller bubbles which are dispersed into the liquid phase. A larger number of bubbles with sizes less than 1mm which were formed in the reactor have high interfacial area which results in a high gas-liquid mass transfer rate.

2.6.4 Effect of reactor parameters and reactor design

The structure and design of reactors influence the fluid flow pattern observed, causing flow separation or eddy occurrence. Thus the reactor characteristics represent another aspect which plays a role in understanding the mass transfer inside the reactor.

Zhang analyzed the mass transfer capability of a corrugated plate photoreactor compared with a flat plate reactor in wastewater treatment applications [76]. In this study, the mass transfer coefficient was measured at different corrugation angles for corrugated plates, as well as at different flow rates. It was found that the smaller corrugation angle used in the corrugated plates corresponded to a higher mass transfer rate over that of the flat plate.

Trujillo et al. analyzed the mass transfer processes which occur in a multiphase tank reactor containing submerged coated inclined-plates [77]. Different orientations of the plate were chosen to computationally and experimentally determine the optimum angle of plate inclination for enhanced mass transfer rate. It was found that the mass transfer coefficient was higher with the inclined plate than with the vertical or horizontal orientation and an optimum inclination angle of 38.6 for the TiO_2 coated plate was found for application of the photoreactor to solar wastewater treatment.

2.7 Mass transfer limitations within photocatalytic reactors

Photocatalytic reactors for water treatment have been developed over the past 30 years. Many challenges are involved in the design of efficient photocatalytic reactors, which vary from classical chemical reactor designs in that process considerations such as distribution

and modeling of light sources, sufficient mass transfer capacity, and high exposed surface area for catalyst per unit reactor volume must be thoroughly investigated, in addition to operational parameters. A wide variety of photocatalytic novel reactor configurations designed to improve mass transfer and maximize irradiation for photocatalysis been published including: the annular photoreactor, rotating disc photoreactor, swirl flow reactor, and so on. They can be classified into two main categories based on the state of the photocatalyst, namely the suspended and immobilized configurations, respectively. In suspension or slurry systems, the catalyst is suspended in the liquid phase, leading to a high total surface area of photocatalyst per unit volume. However, the separation of the catalyst particles is difficult and expensive. The second approach is to attach the catalyst to a transparent stationary support as immobilized catalyst system, where the photocatalyst is immobilized onto an inert carrier. This system is often associated with mass transfer limitations over the catalyst layer. The photocatalyst film thickness may also affect the mass transfer rate. Therefore, mass transfer is an important factor that must be studied in both slurry and immobilized photocatalytic reactors.

2.7.1 Suspension system

Mass transfer limitation influences the rate of photocatalytic reaction within slurry reactors, and is very important for the reaction kinetic analysis and for photoreactor design. Since the mass transfer limitation strongly affects the efficiency of slurry reactors, the mass transfer

phenomena within photoreactors is of interest in many researches.

A kinetic study of photocatalytic degradation in a TiO_2 slurry system was reported to distinguish kinetic and transport limited regimes [78]. The effect of catalyst loading, circulation rate, and initial concentration of solute and light intensity on the degradation rate was analyzed for both monoparameter and multiparameter variation. The results showed that there is no external mass transfer limitation at any catalyst loading, but internal mass transfer limitation and light limitation exist at high catalyst loading conditions.

Ballari et al. investigated the effect of flow rate, catalyst loading, irradiation rates, total suspension volume, virtual changes in kinetic constant and reactor illuminated length, and analyzed the mass transfer limitation within the reactor employing TiO_2 suspensions [79, 80]. The concentration gradients in the bulk solution which caused the mass transfer limitation was found to always exist unless very good mixing conditions were used in the characteristic direction of radiation propagation. These concentration gradients are difficult to avoid in practice, but can be negligible when fully developed turbulent flow is achieved within reactor. The mass transfer limitation can also be ignored at certain values of catalyst loading and incoming irradiation rates. The external and internal mass transfer limitation in photocatalytic suspensions of TiO_2 are analyzed in detail in later studies. It was found that the interfacial mass transport in the boundary layer of catalytic particles could be observed only for large particle sizes, while internal mass transfer limitations in catalyst agglomerates were always present due to the light penetration restrictions. Additionally, the photocatalytic

reaction rate was found to be affected by mass and photon transfer restrictions inside the particle agglomeration of TiO_2 [81]. This was due to the radiation transfer constraints inside the formed agglomerates causing the transfer limitation.

2.7.2 Immobilized system

The use of photocatalyst immobilized over suitable supports in photoreactors has been developed for wastewater treatment. This approach eliminates the need for separation of catalyst particles from the liquid phase post-treatment, and the catalyst film can also provide a large surface area for degradation of contaminants. However, immobilization of catalyst on supports also has some associated disadvantages such as: the effective accessibility to the photocatalyst surface of both photons and reactants, and the influence of increasing photocatalyst film thickness to the internal mass transfer leading to a limited utilization of the catalyst material near the support-catalyst interface. All these factors result in a lower degradation rate of contaminants in immobilized photocatalyst systems.

Dionysiou et al. investigated the effect of disk angular velocity, contaminant concentration, and incident light intensity on the degradation of 4-chlorobenzoic acid and mass transfer limitations in a rotating disk photoreactor [73]. The results obtained indicated that the photocatalytic reaction rates increased rapidly with disk angular velocity in the range of 2-6 rpm due to the existence of mass transfer limitations. Above 6 rpm, the significant mass transfer limitations disappeared and the reaction rates were mainly controlled by surface

reaction.

McMurray et al. reported the degradation of oxalic acid and formic acid in a stirred tank reactor with immobilized TiO_2 [82]. It was found that mass transfer did not limit the rate of photocatalytic reaction of either acid at propeller speeds greater than 1000 rpm.

An annular TiO_2-supported reactor for photocatalytic oxidation of paint solvent compounds in air was developed by Palau et al. [83]. However, no mass transfer limitation was found under the experimental conditions. Another study of photocatalytic degradation of acetone in an annular reactor was performed by CFD modeling [84], and neither external mass transfer nor internal diffusion limitations were observed. Lim et al. also used an annular photoreactor with TiO_2 adsorbed on a quartz tube for decomposition of phenanthrene [85]. They indicated that the chemical reaction controlled the process when the velocity was greater than 7 cm/min and thus no mass transfer limitation occurred.

Another study of indoor air purification was performed by using formaldehyde as target pollutant and immobilized nanometer TiO_2 particles on the surface of an activated carbon (AC) to explore the influence of mass transfer [86]. It was found that the photocatalytic reaction rate increased with the increase of flow velocity in the mass transfer controlled process, while it changed little in the photocatalytic reaction controlled process. The critical point of the photocatalytic reaction from the mass transfer controlled process to the photocatalytic reaction controlled process was ahead by the TiO_2/AC film compared with the results by the TiO_2/glass film.

Zhang et al. developed a corrugated plate reactor for degradation of 4-chlorophenol and described its performance compared to a flat plate reactor and a slurry reactor [87, 88]. The mass transfer limitation was observed in both flat plate reactor and corrugated plate reactor. The overall mass transfer conditions could be improved in the corrugated plates with a small degree of corrugation, but the limitation could never be eliminated. It was also found that the mass transfer rates in corrugated plate reactors were up to 600% higher than those in the flat plate reactors.

Dijkstra et al. developed a kinetic model for the photocatalytic degradation of formic acid in an immobilized system and investigated the mass transfer processes within the tubular reactor [89]. Various gas and liquid flow rates were operated to study the influence of external mass transport. It was found that mass transfer limitations existed due to the degradation rates of formic acid increasing with increasing flow rate. They also compared the degradation rate observed with different catalyst configurations such as in: a suspended system, an immobilized system with a coated wall, and an immobilized system packed with coated glass beads [90]. It found that the mass transfer limitation only occurred in the reactor with the catalyst coated on the wall and the degradation rate could be improved by the addition of air directly in this reactor due to the decreased mass transfer limitation.

Mass transfer limitations exist in most immobilized photocatalytic reactors. The reduction of the impact of mass transfer on the degradation rate is an important issue in photocatalysis studies. The most efficient way to achieve this is in the improvement of fluid flow velocity,

which directly increases the mass transfer rate. Changing the film thickness of photocatalyst is another method to influence the internal mass transfer. Additionally, different constructions of photocatalytic reactors also lead to different reaction rates. In order to obtain better results from photocatalytic studies, every factor that affects the mass transfer process should be considered.

2.8 Conclusions

Photocatalysis is a process which has been developed and studied for the past few decades and possesses a good capacity and applicability for use in the waste treatment. However, mass transfer limitations in photocatalytic reaction seriously influence the degradation of contaminants. The researches of mass transfer processes in photocatalytic reactors are discussed and analyzed in this review.

The various methods used for the measurement of mass transfer coefficients are considered in attempt to address their advantages and disadvantages. The dissolution method is the most widely used, and measures the average liquid-solid mass transfer coefficient with simplest operation at atmosphere condition. However, the coated solid may dissolve into the liquid phase before the experiment begins and be lost when flashing or stripping occurs. The naphthalene sublimation method for the measurement of gas-solid mass transfer is a good way to obtain the heat transfer coefficient through transport analogues. However, the depleted naphthalene layer may lead to error in results. The electrochemical method has a

great accuracy that measures the liquid-solid mass transfer coefficient with controlled driving force. The decomposition of electrolyte, however, would precipitate onto the surface of electrodes reducing the limiting current. The absorption method measures the gas-side mass transfer coefficient or liquid-side mass transfer coefficient by controlling the gas absorption rate, however, the various interfacial area of gas and liquid and concentration of liquid phase should be focused on in order to reduce the experimental error.

Computational fluid dynamic modeling is another indispensable tool to simulate and predict the fluid flow pattern and mass transfer process. Turbulence models based on Reynolds-averaged Navier-Stokes equations are often adopted. SST k-ω model is recommended to be the first choice instead of k-ε model.

Some of the factors that affect the mass transfer rate have been reviewed. In order to overcome mass transfer limitations, improving the fluid flow rate, rotational speed or agitating speed of reactors has shown to be technically feasible. The geometric design of reactors may also be altered, such as in the corrugated angle reactor. The orientation of plate reactors has also been investigated with respect to mass transfer, and is another aspect for the investigation of mass transfer limitations.

For both suspended and immobilized photocatalytic systems, the research on mass transfer limitation is necessary because reduction of external and internal mass transfer limitations to the photocatalytic reaction enhances the degradation of contaminants.

In conclusion, studying the mass transfer aspects to photocatalytic reactions is an important

factor which can contribute to better understanding of this AOP for use in waste treatment.

2.9 References

[1] S. Malato, P. Fernández-Ibáñez, M.I. Maldonado, J. Blanco, W. Gernjak, Decontamination and disinfection of water by solar photocatalysis: Recent overview and trends, Catalysis Today, 147 (2009) 1-59.

[2] M. Kositzi, I. Poulios, S. Malato, J. Cáceres, A. Campos, Solar photocatalytic treatment of synthetic municipal wastewater, Water Research, 38 (2004) 1147-1154.

[3] R.S. Ramalho, Introduction to wastewater treatment processes, Academic Press, 1977.

[4] P.V.A. Padmanabhan, K.P.Sreekumar, T.K. Thiyagarajan, R.U. Satpute, Nano-crystalline titanium dioxide formed by reactive plasma synthesis, Vacuum 80 (2006) 11-12.

[5] W.Glaze, J.W. Kang, D. H. Chapin, The Chemistry of Water Treatment Processes Involving Ozone, Hydrogen Peroxide and Ultraviolet Radiation, Ozone: Science & Engineering: The Journal of the International Ozone Association 9 (1987) 335–352.

[6] A.K. Ray, Photocatalytic reactor configurations for water purification: experimentation and modeling, Advances in Chemical Engineering, 36 (2009) 145-184.

[7] X. Wang, K. Maeda, A. Thomas, K. Takanabe, G. Xin, J.M. Carlsson, K. Domen, M. Antonietti, A metal-free polymeric photocatalyst for hydrogen production from water under visible light, Nature materials, 8 (2008) 76-80.

[8] A.L. Linsebigler, G. Lu, J.T. Yates Jr, Photocatalysis on TiO_2 surfaces: principles,

mechanisms, and selected results, Chemical Reviews, 95 (1995) 735-758.

[9] R.J. Braham, A.T. Harris, Review of major design and scale-up considerations for solar photocatalytic reactors, Industrial and Engineering Chemistry Research, 48 (2009) 8890-8905.

[10] M.N. Chong, B. Jin, C.W.K. Chow, C. Saint, Recent developments in photocatalytic water treatment technology: A review, Water Research, 44 (2010) 2997-3027.

[11] T.L. Bergman, F.P. Incropera, A.S. Lavine, D.P. DeWitt, Fundamentals of heat and mass transfer, John Wiley & Sons, 2011.

[12] D.R. Gabe, D.J. Robinson, Mass transfer in a rotating cylinder cell-II. turbulent flow, Electrochimica Acta, 17 (1972) 1129-1137.

[13] M. Jin Kim, Y. Sung Ghim, H. Nam Chang, Oxygen transfer in a rotating disk reactor with continuous flow, Chemical Engineering Science, 40 (1985) 2281-2286.

[14] W.J. Korchinsky, A.M. Ismail, Mass-transfer parameters in rotating-disc contactors: Influence of column diameter, Journal of Chemical Technology and Biotechnology, 43 (1988) 147-158.

[15] A. Aoune, C. Ramshaw, Process intensification: Heat and mass transfer characteristics of liquid films on rotating discs, International Journal of Heat and Mass Transfer, 42 (1999) 2543-2556.

[16] E. Nelson, Dynamical theories of Brownian motion, Princeton university press Princeton, 1967.

[17] C.O. Bennett, J.E. Myers, Momentum, heat, and mass transfer, McGraw-Hill New York, 1982.

[18] Private pilot ground school, Airplane aerodynamics: fundamentals and flight principles, http://www.free-online-private-pilot-ground-school.com/aerodynamics.html, 2006.

[19] Jules Thibault, Advanced Transport Phenomena, University of Ottawa, Canada, 2010.

[20] Z. Zhang, X. Deng, Y. Fan, R. Guidoin, The effects of recirculation flows on mass transfer from the arterial wall to flowing blood, ASAIO Journal, 54 (2008) 37-43.

[21] E. Kaunisto, B. Nilsson, A. Axelsson, Drug dissolution rate measurements evaluation of the rotating disc method, Pharmaceutical Development and Technology, 14 (2009) 400-408.

[22] U.K. Ghosh, S. Kumar, S.N. Upadhyay, Mass transfer from spherical and nonspherical particles to non-Newtonian fluids, Polymer-plastics technology and engineering, 31 (1992) 271-290.

[23] R.V. Garić-Grulović, Ž.B. Grbavčić, N. Bošković-Vragolović, Z.L. Arsenijević, Mass transfer in vertical liquid-solids flow of coarse particles, Powder Technology, 189 (2009) 130-136.

[24] J. Chen, X. Yang, J.M. Yu, Y.F. Jiang, J.M. Chen, Investigation of effect and process of nitric oxide removal in rotating drum biofilter coupled with absorption by Fe II(EDTA), Huanjing Kexue/Environmental Science, 33 (2012) 539-544.

[25] A. W. Hixson, S. J. Baum, Mass Transfer Coefficients in Liquid-Solid Agitated Systems, Eng. Chem., 33 (1941) 478.

[26] M.H. Abdel-Aziz, I.A.S. Mansour, G.H. Sedahmed, Study of the rate of liquid–solid mass transfer controlled processes in helical tubes under turbulent flow conditions, Chemical Engineering and Processing: Process Intensification, 49 (2010) 643-648.

[27] I. Pitault, P. Fongarland, D. Koepke, M. Mitrovic, D. Ronze, M. Forissier, Gas-liquid and liquid-solid mass transfers in two types of stationary catalytic basket laboratory reactor, Chemical Engineering Science, 60 (2005) 6240-6253.

[28] M. Winterbottom, R. Fishwick, H. Stitt, Solid-liquid mass transfer and hydrodynamics in the hydrogenation of 4-nitrobenzoic acid, Canadian Journal of Chemical Engineering, 81 (2003) 588-596.

[29] R.J.P.S. R. Tschentscher, T. A. Nijhuis, J. van der Schaaf, and J. C. Schouten, Liquid-Solid Mass Transfer in Agitated Slurry Reactors and Rotating Solid, Ind. Eng. Chem. Res. , 49 (2010) 10758–10766.

[30] M. Al-Dahhan, W. HighFill, B.T. Ong, Drawbacks of the dissolution method for measurement of the liquid-solid mass-transfer coefficients in two-phase flow packed-bed reactors operated at low and high pressures, Industrial and Engineering Chemistry Research, 39 (2000) 3102-3107.

[31] P. Souza Mendes, The naphthalene sublimation technique, Experimental Thermal and Fluid Science, 4 (1991) 510-523.

[32] R. Goldstein, H. Cho, A review of mass transfer measurements using naphthalene sublimation, Experimental Thermal and Fluid Science, 10 (1995) 416-434.

[33] H.J. Sung, K.S. Hwang, J.M. Hyun, Experimental study on mass transfer from a circular cylinder in pulsating flow, International Journal of Heat and Mass Transfer, 37 (1994) 2203-2210.

[34] S.C. Roh, S.O. Park, Surface flow pattern and local mass transfer on the free-end surface of a finite circular cylinder, Heat and Mass Transfer, 38 (2002) 1-5.

[35] K. Ghosh, R.J. Goldstein, Investigation of flow and mass transfer on a flat plate downstream of a shear inducing moving wall, ASME, (2010) 467-475.

[36] H.G. Kwon, S.D. Hwang, H.H. Cho, Measurement of local heat/mass transfer coefficients on a dimple using naphthalene sublimation, International Journal of Heat and Mass Transfer, 54 (2011) 1071-1080.

[37] J.H. Park, S.Y. Yoo, A naphthalene sublimation study on heat/mass transfer for flow over a flat plate, KSME International Journal, 18 (2004) 1258-1266.

[38] S.Y. Yoo, W.S. Jo, W.S. Cho, An experimental study of local mass transfer characteristics on inclined flat plate, Transactions of the Korean Society of Mechanical Engineers, B, 35 (2011) 1335-1341.

[39] J.P. Brakell, T.A. Cowell, An analysis of the uniform naphthalene layer mass treansfer analogue method applied to laminar flow over a flat plate, 8th International Heat Transfer Conference, 2 (1986) 495-499.

[40] J.R. Burns, R.J.J. Jachuck, Determination of liquid-solid mass transfer coefficients for a spinning disc reactor using a limiting current technique, International Journal of Heat and

Mass Transfer, 48 (2005) 2540-2547.

[41] H. Xu, W. Huang, Y. Xing, H. Lin, H. Ji, M. Jiang, X. Liu, S. Gan, Effect of Configuration on Mass Transfer in a Filter-press Type Electrochemical Cell* * Supported by the National Natural Science Foundation of China (20573045, 20843001), the "Tenth Five-Year" National Key Scientific and Technological Project (2004BA313B-17) and the National High Technology Research and Development Program of China (2006AA06Z321), Chinese Journal of Chemical Engineering, 16 (2008) 198-202.

[42] J. Su, H.Y. Lu, H. Xu, J.R. Sun, J.L. Han, H.B. Lin, Mass transfer enhancement for mesh electrode in a tubular electrochemical reactor using experimental and numerical simulation method, Russian Journal of Electrochemistry, 47 (2011) 1293-1298.

[43] R. Xu, H. Fei, P. Zhu, H. Gu, Measurement of enhanced mass transfer coefficient in tube by limiting diffusion current technique, Shiyou Huagong/Petrochemical Technology, 36 (2007) 712-715.

[44] K.U. Kang, B.J. Chung, The effects of the anode size and position on the limiting currents of natural convection mass transfer experiments in a vertical pipe, Transactions of the Korean Society of Mechanical Engineers, B, 34 (2010) 1-8.

[45] G. Weyns, G. Nelissen, J.G.A. Pembery, P. MacIel, J. Deconinck, H. Deconinck, M.A. Patrick, A.A. Wragg, Turbulent fluid flow and electrochemical mass transfer in an annular duct with an obstruction, Journal of Applied Electrochemistry, 39 (2009) 2453-2459.

[46] M.H. Abdel-Aziz, Mass transfer behavior at horizontal cylinder in cross flow under

different flow conditions, International Communications in Heat and Mass Transfer, 38 (2011) 493-498.

[47] P. Coñizares, J. García-Gómez, I. Fernández de Marcos, M.A. Rodrigo, J. Lobato, Measurement of mass-transfer coefficients by an electrochemical technique, Journal of Chemical Education, 83 (2006) 1204-1207.

[48] J. Gostick, H.D. Doan, A. Lohi, M.D. Pritzker, Investigation of local mass transfer in a packed bed of Pall rings using a limiting current technique, Industrial and Engineering Chemistry Research, 42 (2003) 3626-3634.

[49] N.J.R. Kraakman, J. Rocha-Rios, M.C.M. Van Loosdrecht, Review of mass transfer aspects for biological gas treatment, Applied Microbiology and Biotechnology, 91 (2011) 873-886.

[50] J. Yue, G. Chen, Q. Yuan, L. Luo, Y. Gonthier, Hydrodynamics and mass transfer characteristics in gas-liquid flow through a rectangular microchannel, Chemical Engineering Science, 62 (2007) 2096-2108.

[51] Y. Fan, R.K. Herz, Measurement and enhancement of gas-liquid mass transfer in milliliter-scale slurry reactors, Chemical Engineering Science, 62 (2007) 5940-5951.

[52] W. Last, J. Stichlmair, Determination of mass transfer parameters by means of chemical absorption, Chem Eng Technol, 25 (2002) 385–391.

[53] A. Hoffmann, J.F. Maćkowiak, A. Górak, M. Haas, J.M. Löning, T. Runowski, K. Hallenberger, Standardization of Mass Transfer Measurements. A Basis for the Description

of Absorption Processes, Chemical Engineering Research and Design, 85 (2007) 40-49.

[54] A.M. Dehkordi, C. Savari, Determination of interfacial area and overall volumetric mass-transfer coefficient in a novel type of two impinging streams reactor by chemical method, Industrial and Engineering Chemistry Research, 50 (2011) 6426-6435.

[55] P.R. Gogate, A.B. Pandit, Survey of measurement techniques for gas-liquid mass transfer coefficient in bioreactors, Biochemical Engineering Journal, 4 (1999) 7-15.

[56] Andersson B., Andersson R., Hakansson L., Mortensen M., Sudiyo R., Wachem B V., Computational Fluid Dynamics for Engineers, Cambridge, 2012.

[57] H.K. Versteeg, W. Malalasekera, An introduction to computational fluid dynamics: the finite volume method, Prentice Hall, 2007.

[58] J.D. Anderson, Computational fluid dynamics, McGraw-Hill New York, 1995.

[59] M.A. Leon, R.J. Maas, A. Bieberle, M. Schubert, T.A. Nijhuis, J. van der Schaaf, U. Hampel, J.C. Schouten, Hydrodynamics and gas-liquid mass transfer in a horizontal rotating foam stirrer reactor, Chemical Engineering Journal, 217 (2013) 10-21.

[60] M.K. Moraveji, B. Sajjadi, M. Jafarkhani, R. Davarnejad, Experimental investigation and CFD simulation of turbulence effect on hydrodynamic and mass transfer in a packed bed airlift internal loop reactor, International Communications in Heat and Mass Transfer, 38 (2011) 518-524.

[61] C.E. Zambra, C. Rosales, N.O. Moraga, M. Ragazzi, Self-heating in a bioreactor: Coupling of heat and mass transfer with turbulent convection, International Journal of Heat

and Mass Transfer, 54 (2011) 5077-5086.

[62] Y. Zhang, E.K. Stefanakos, D. Yogi Goswami, Effect of photocatalytic surface roughness on reactors effectiveness for indoor air cleaning, Building and Environment, 61 (2013) 188-196.

[63] J. Esteban Duran, F. Taghipour, M. Mohseni, CFD modeling of mass transfer in annular reactors, International Journal of Heat and Mass Transfer, 52 (2009) 5390-5401.

[64] A. Cockx, Z. Do-Quang, J.M. Audic, A. Liné, M. Roustan, Global and local mass transfer coefficients in waste water treatment process by computational fluid dynamics, Chemical Engineering and Processing, 40 (2001) 187-194.

[65] L. Rong, P.V. Nielsen, G. Zhang, Experimental and numerical study on effects of airflow and aqueous ammonium solution temperature on ammonia mass transfer coefficient, Journal of the Air and Waste Management Association, 60 (2010) 419-428.

[66] W. Huang, C. Wu, W. Xia, Oxygen transfer in high-speed surface aeration tank for wastewater treatment: Full-scale test and numerical modeling, Journal of Environmental Engineering, 135 (2009) 684-691.

[67] X. Wang, X. Jia, J. Wen, Transient CFD modeling of toluene waste gas biodegradation in a gas-liquid-solid three-phase airlift loop reactor by immobilized Pseudomonas putida, Chemical Engineering Journal, 172 (2011) 735-745.

[68] R. Bannari, A. Bannari, B. Selma, P. Proulx, Mass transfer and shear in an airlift bioreactor: Using a mathematical model to improve reactor design and performance,

Chemical Engineering Science, 66 (2011) 2057-2067.

[69] Koide K, Horibe K, Kawabata H and Ito S, Gas holdup and volumetric liquid phase mass transfer coefficient in solid suspended bubble column with draught tube, Chem. Eng. Jpn. 18 (1985) 248–253.

[70] K. Muthukumar, Volumetric mass transfer coefficients in an internal loop airlift reactor with low-density particles, Journal of Chemical Technology and Biotechnology, 81 (2006) 667–673.

[71] D. Chen, F. Li, A.K. Ray, Effect of mass transfer and catalyst layer thickness on photocatalytic reaction, AIChE Journal, 46 (2000) 1034-1045.

[72] C. McCullagh, N. Skillen, M. Adams, P.K.J. Robertson, Photocatalytic reactors for environmental remediation: a review, Journal of Chemical Technology & Biotechnology, 86 (2011) 1002-1017.

[73] D.D. Dionysiou, M.T. Suidan, I. Baudin, J.M. Laîné, Oxidation of organic contaminants in a rotating disk photocatalytic reactor: Reaction kinetics in the liquid phase and the role of mass transfer based on the dimensionless Damköhler number, Applied Catalysis B: Environmental, 38 (2002) 1-16.

[74] N.A. Hamill, L.R. Weatherley, C. Hardacre, Use of a batch rotating photocatalytic contactor for the degradation of organic pollutants in wastewater, Applied Catalysis B: Environmental, 30 (2001) 49-60.

[75] R. Rakoczy, S. Masiuk, Influence of transverse rotating magnetic field on enhancement

of solid dissolution process, AIChE Journal, 56 (2010) 1416-1433.

[76] Z. Zhang, Analysis of a corrugated-plate photocatalytic reactor, Ph.D. Thesis, University of Waterloo, Canada, 1999.

[77] F.J. Trujillo, T. Safinski, A.A. Adesina, Solid–liquid masstransfer analysis in a multi-phase tank reactor containing submerged coated inclined-plates: A computational fluid dynamics approach, Chemical Engineering Science, 42 (2009) 1143-1153.

[78] K. Mehrotra, G.S. Yablonsky, A.K. Ray, Kinetic studies of photocatalytic degradation in a TiO_2 slurry system: Distinguishing working regimes and determining rate dependences, Industrial and Engineering Chemistry Research, 42 (2003) 2273-2281.

[79] M.d.l.M. Ballari, R. Brandi, O. Alfano, A. Cassano, Mass transfer limitations in photocatalytic reactors employing titanium dioxide suspensions. I. Concentration profiles in the bulk, Chemical Engineering Journal, 136 (2008) 50-65.

[80] M.d.l.M. Ballari, R. Brandi, O. Alfano, A. Cassano, Mass transfer limitations in photocatalytic reactors employing titanium dioxide suspensions. II. External and internal particle constrains for the reaction, Chemical Engineering Journal, 136 (2008) 242-255.

[81] M.d.l.M. Ballari, O.M. Alfano, A.E. Cassano, Mass transfer limitations in slurry photocatalytic reactors: Experimental validation, Chemical Engineering Science, 65 (2010) 4931-4942.

[82] T.A. McMurray, J.A. Byrne, P.S.M. Dunlop, J.G.M. Winkelman, B.R. Eggins, E.T. McAdams, Intrinsic kinetics of photocatalytic oxidation of formic and oxalic acid on

immobilised TiO_2 films, Applied Catalysis A: General, 262 (2004) 105-110.

[83] J. Palau, J.M. Penya-Roja, C. Gabaldón, F. Javier Álvarez-Hornos, F. Sempere, V. Martínez-Soria, UV photocatalytic oxidation of paint solvent compounds in air using an annular TiO_2-supported reactor, Journal of Chemical Technology and Biotechnology, 86 (2011) 273-281.

[84] G. Vincent, E. Schaer, P.M. Marquaire, O. Zahraa, CFD modelling of an annular reactor, application to the photocatalytic degradation of acetone, Process Safety and Environmental Protection, 89 (2011) 35-40.

[85] T.H. Lim, S.D. Kim, Photocatalytic degradation of trichloroethylene (TCE) over TiO_2/silica gel in a circulating fluidized bed (CFB) photoreactor, Chemical Engineering and Processing: Process Intensification, 44 (2005) 327-334.

[86] Y. Lu, D. Wang, C. Ma, H. Yang, Study on the effect of mass transfer on the photocatalytic removal of formaldehyde, Proceedings of the Inaugural US-EU-China Thermophysics Conference, 2009.

[87] Z. Zhang, W. Anderson, M. Mooyoung, Experimental analysis of a corrugated plate photocatalytic reactor, Chemical Engineering Journal, 99 (2004) 145-152.

[88] Z. Zhang, W.A. Anderson, M. Moo-Young, Modeling of corrugated plate photocatalytic reactors and experimental validation, Chemical Engineering Science, 58 (2003) 911-914.

[89] M.F.J. Dijkstra, H.J. Panneman, J.G.M. Winkelman, J.J. Kelly, A.A.C.M. Beenackers, Modeling the photocatalytic degradation of formic acid in a reactor with immobilized

catalyst, Chemical Engineering Science, 57 (2002) 4895-4907.

[90] M.F.J. Dijkstra, H. Buwalda, A.W.F. De Jong, A. Michorius, J.G.M. Winkelman, A.A.C.M. Beenackers, Experimental comparison of three reactor designs for photocatalytic water purification, Chemical Engineering Science, 56 (2001) 547-555.

CHAPTER 3

Experimental and computational analysis of mass transfer phenomena in a corrugated photoreactor

Abstract

Experimental and computational investigations of mass transfer processes in corrugated photocatalytic reactors were conducted. The effects of various parameters such as drum rotational speed, reactor liquid volume and number of corrugations on mass transport phenomena were investigated. The results indicated that the mass transfer rate increased with increasing rotational speed from 5 rpm to 80 rpm. Additionally, using liquid volume which immersed 20% of the corrugated drum surface area was found to significantly impact mass transfer. The drum with 28 corrugations provided the most efficient mass transfer rate, and exhibited the lowest mass transfer coefficient of all of the configurations studied. Computational fluid dynamic simulations were carried out for each of the experimental geometries to explore the physical mechanisms of the mass transfer process. Mass transfer limitations between the corrugation volume and the bulk solution resulted in a lower observed mass transfer coefficient from the simulation compared to the experimental results.

Keywords: *photoreactor, corrugated drum, mass transfer, simulation, CFD*

3.1 Introduction

Photocatalysis has been widely considered for the treatment of environmental pollutants, specifically for air and wastewater purification [1]. Since photocatalytic reactions have the ability to oxidize the organic compounds completely to carbon dioxide by UV light, it is considered both clean and green technology [2]. An increasing number of publications in this field have attempted to develop ways to improve the contaminant degradation effect of photocatalytic reactions and apply this technology at scales relevant to an industrial treatment system.

Two distinct areas of study exist for the photocatalysis for remediation of polluted water [3]: identification and characterization of photocatalytic materials with superior capabilities to decompose [4-6]; and the design of efficient reactors which optimize both utilization of the light source and distribution of contaminants [7-12]. A technically and economically effective photocatalytic reactor should ideally possess a large catalyst surface area per unit reactor volume, the ability for the catalyst to recapture photons reflected from the catalyst surface, and the sufficient mass transfer capacity between the liquid bulk and the reacting sites [13].

The coupling between both catalytic activity from UV exposure and mass transfer presents challenges both in simulating reactor performance and designing experimental systems, which has led to several literature sources analyzing mass transfer effects on photocatalytic reactions and reactors. For instance, Chen et al. investigated the effect of mass transfer and

catalyst layer thickness on photocatalytic degradation of benzoic acid over Degussa P25 TiO_2 thin film supported on a Pyrex glass substrate [14]. It was found that the internal mass transfer, which was determined by the performance of catalyst, coating methods and the thickness of the catalyst film, was an intrinsic property of the catalyst film and its resistance could control the overall mass transfer rate, while the external mass transfer resistance could be neglected by increasing the Reynolds number of the flowing solution [15]. Ballari et al. explored a model that could predict the appearance of mass transfer limitations under certain operating conditions of a slurry photocatalytic reactor that affects degradation rate of the contaminant [16]. The reaction rate in a transient, two-dimensional mass balance condition was affected by an effectiveness factor considering mass and photon transfer restrictions inside the particle agglomeration of TiO_2. The reduction in irradiated area within agglomerates of TiO_2 particles was identified as a significant factor which leads to the appearance of mass transfer limitations. Dionysiou et al. investigated the effect of disk angular velocity, contaminant concentration, and incident light intensity on the degradation of 4-chlorobenzoic acid and mass transfer limitations in a rotating disk photoreactor [17]. The results obtained indicated that the photocatalytic reaction rates increased rapidly with disk angular velocity in the range of 2-6 rpm due to the existence of mass transfer limitations. Above 6 rpm, the significant mass transfer limitations disappeared and the reaction rates were mainly controlled by surface reaction. McMurray et al. reported the degradation of oxalic acid and formic acid in a stirred tank reactor with immobilized TiO_2 films on a glass

plate [18], determining that mass transfer did not limit the rate of photocatalytic reaction at propeller rotation speeds above 1000 rpm. An annular TiO_2-supported reactor for photocatalytic oxidation of paint solvent compounds in air was developed by Palau et al. [19]. However, no mass transfer limitation was found under the experimental conditions. Another study of photocatalytic degradation of acetone in an annular reactor was performed by CFD modeling, and neither external mass transfer nor internal diffusion limitations were observed [20]. Lim et al. also used an annular photoreactor with TiO_2 adsorbed on a quartz tube for decomposition of phenanthrene [21]. They indicated that the chemical reaction controlled the process when the velocity was greater than 7 cm/min, with limited mass transfer limitation observed.

A novel photocatalytic reactor consisting of a corrugated surface was designed to increase the efficiency of photocatalytic reactions [22-25]. The corrugated surface not only increased the catalyst immobilization surface area per unit reactor volume but also had the potential to recapture reflected light and result in higher photon absorption efficiency [26, 27]. The capacity for transport of pollutants in corrugated plate photocatalytic reactor was found to be 400%-600% higher than comparable flat plate reactors. The angle of the corrugated plate photocatalytic reactor significantly affected the local-area-specific rate of energy absorption and the energy absorption efficiency [28].

A stationary corrugated reactor, however, typically experienced mass transfer limitations and significant attenuation of incident UV energy when submerged in practical fluids of interest.

To overcome this, rotating corrugated reactors were proposed whereby a corrugated drum was partially immerged in the solution and other side was exposed to air and a UV light source. The photocatalytic reactions occurred only at the upper part of the reactor within a thin film of polluted water carried by the corrugations during the rotation in the presence of photocatalyst, UV radiation, and oxygen from the atmosphere [29].

Several degradation experiments have been reported for the TiO_2 coated corrugated photocatalytic reactors [30, 31]. The effects of different corrugation angles, rotating speeds, initial pollutant concentrations, and illumination intensities were investigated. Although, the different angles and surface area of the corrugated reactors had little effect on the degradation of phenol solution, the large corrugated surface area increased the degradation rate up to 200% compared to previous reports for annular reactor configurations. In this previous work, operation at low concentrations of contaminants (5 ppm) were found to be mass transfer limited, with significant dependencies between reactor performance and rotation rate. In contrast, high concentrations of contaminants (20-40 ppm) appeared to result in kinetic limitations, with the rotation rate not having as large of an effect.

Computational analysis of a comparable system treating methylene blue (MB) attempted to further study local coupling effects between the spatial distribution of incident energy within an actual experimental system and reactor performance [32]. In their work, radiation patterns including incident energy distribution and local area-specific rates of energy absorption were simulated for an actual light-box configuration using finite-element discrete-ordinate models,

and were subsequently applied to the rotating corrugated geometry. The simulated results of MB decomposition are consistent with experimental data with deviations resulting from the bubble formation on the surface of the reactor at higher rotation speed. Through the numerical analysis, it is also found that the submersion depth and time available to refresh the thin-film pollutant concentration had significant impact on the MB degradation rate. In order to further understand the characteristics of this novel corrugated photoreactor, mass transfer phenomena in the corrugated construction is studied in this work through experimental observation and computational analysis. Three corrugated geometries were considered to explore the influence of the rotational speed, submersion level and bubble formation on mass transfer rate. The flow patterns for different corrugated geometries were also examined in an attempt to determine the applicability of flat-plate mass transfer correlations when simulating the performance of this system.

3.2 Experimental System

3.2.1 Photocatalytic reactors

Mass transfer measurements were performed on the photoreactor system without illumination (Figure 3.1). The drum and the reactor tank were both made of stainless steel. The axis of the drum was connected with a 12V DC gear-motor (Acklands-Grainger, Ontario, Canada). The corrugations of the reactor were coated with benzoic acid and partially immersed in a temperature controlled water reservoir at 20°C, where the change in

concentration of dissolved benzoic acid was monitored over time for specific drum rotational rates.

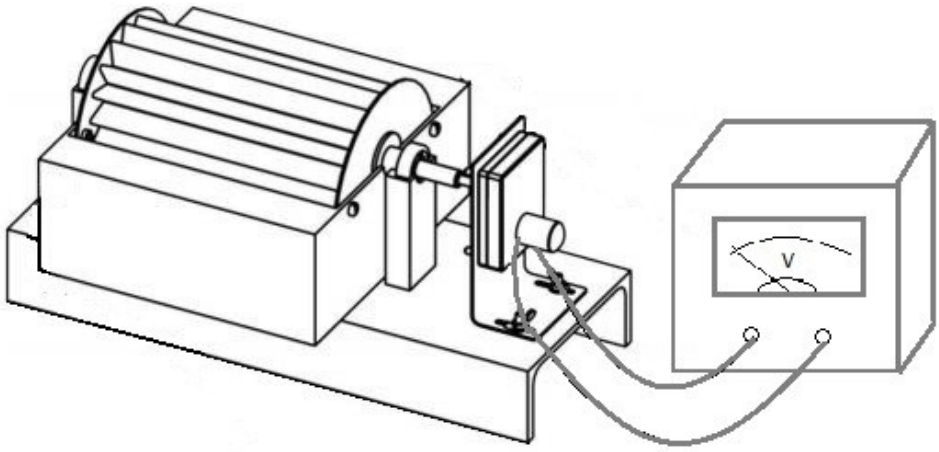

Figure 3.1 Photoreactor experimental apparatus

Three drums were studied in this experiment: 13 corrugations with a 60° corrugation angle; 16 corrugations with a 50° corrugation angle; and 28 corrugations a with 30° corrugation angle. Each drum was constructed with a cylindrical core 6.4 cm in diameter and 20.3 cm in length, with 2 cm high corrugations (Figure 3.2).

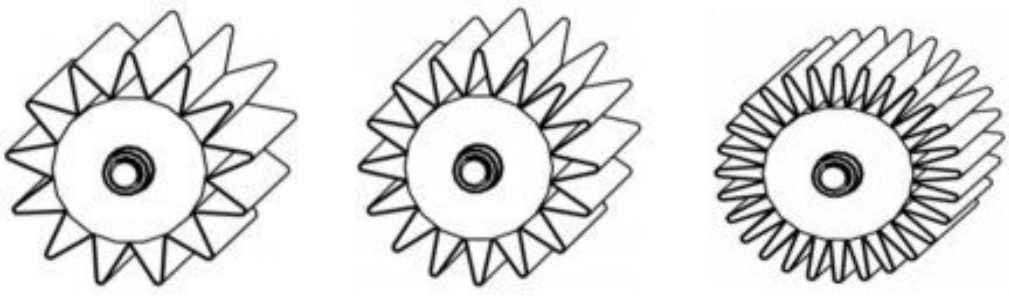

(a) 60°(13C) (b) 50°(16C) (c) 30°(28C)

Figure 3.2 Reactor drums

3.2.2 Methods

The benzoic acid dissolution method was adopted to measure the mass transfer coefficient [33]. Reagent ACS benzoic acid from Fisher Scientific, Canada and deionized water were used in this experiment. Before each test, the drum was heated to 140°C for 3 hours to allow the molten benzoic acid to adhere to its surface before solidifying. The corrugations were then coated with a thin layer of molten benzoic acid using a stainless steel bristle brush (VWR Int.). After coating, the drum was allowed to cool down in air at ambient conditions prior to being submerged in the reservoir during testing.

In preparation for each experimental run, the coated drum and reactor tank were rinsed with deionized water to make sure that there was no detached benzoic acid solid on the drum and no benzoic acid in the tank. The mass transfer studies for each reactor configuration were performed using three reservoir water volumes, V = 1 L, 1.3 L, and1.6 L; and four different rotational speeds, n = 5 rpm, 20 rpm, 50 rpm, and 80 rpm. The three volumes listed corresponded to submersion depths of 19.2%, 31.1% and 44.9% of the drum's total diameter, respectively. Samples of the solution were taken near the wall of the tank every ten minutes and the concentrations of benzoic acid were analyzed with a GENYSYS 10-UV spectrophotometer (Geneq Inc., Quebec, Canada). The concentration was measured at 228 nm which is the highest absorbance peak for benzoic acid and compared with a calibration curve, shown in Figure 3.3. The sample of the solution was diluted 100 times and completely mixed before analysis to minimize the experimental error. The rotational speed of the drum

was controlled during each run via an applied DC voltage. Experiments were carried out until the reservoir was saturated with Benzoic Acid, at which point the surface of the drum was cleaned and the reactor tank was washed. The average mass transfer coefficient was then determined from the concentration vs. time data for the geometry's coated area and rotational speed.

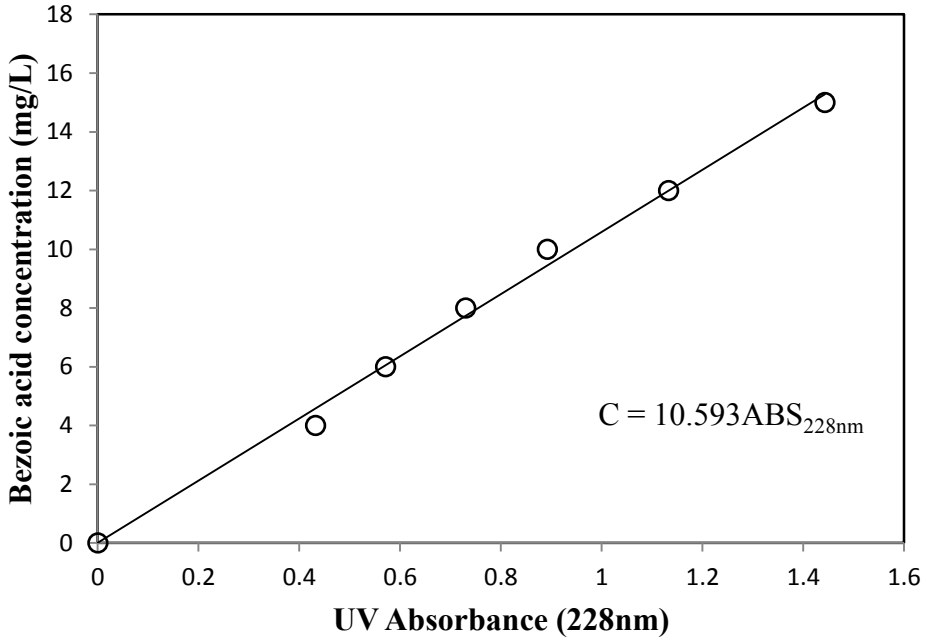

Figure 3.3 Spectrophotometer calibration curve: benzoic acid concentration

A mass balance of benzoic acid within the experimental system can be expressed as:

$$V\frac{dC}{dt} = k_L A(C^* - C) \tag{1}$$

where C^* and C are the dissolved benzoic acid concentrations (g/L) at the liquid side near the solid-liquid interface and in the bulk of the reactor tank, respectively; V is the volume of the water in the tank; A is the area of the drum coated in benzoic acid which is submerged in

water (Table 3.1); k_L is the average mass transfer coefficient. Due to the low solubility of benzoic acid at 20°C (2.9 g/L)[34] and assuming a constant submersed area of the drum, the variation in reservoir concentration with respect to time can be determined through integration of Eq. (1):

$$C(t) = C^* - (C^* - C_0)\, exp\left[\frac{-k_L A(t - t_0)}{V}\right] \quad (2)$$

Where C_0 is the dissolved benzoic acid concentration at time t_0, assumed to be zero. The value of k_L can be determined through least-squares regression of the measured concentration vs. time data.

Table 3.1 Submerged surface area for each drum in different volumes of water

Liquid volume in reservoir	**28C**	**16C**	**13C**
1L	453cm^2	287 cm^2	253 cm^2
1.3L	705 cm^2	508 cm^2	424 cm^2
1.6L	1031 cm^2	656 cm^2	509 cm^2

3.3 CFD modeling

The overall mass transfer coefficient determined from Eq. 2 is a lump-sum model incorporating a number of fluid dynamic and mass transfer mechanisms. Within the experimental system, there is mass transfer between the submerged corrugations and bulk, the coated surface and the thin film present above the reservoir, and in fluid which is

displaced from the reservoir at higher rotation rates. An integrated model applied previously to this system obtained reasonable agreement to experimental data when using a compartmentalized model, to describe different stages in the rotation process [13, 30]. There was, however, a significant mass transfer limitation observed between the submerged surface and bulk fluid based on the application of mass transfer correlations for an idealized flat-plate geometry. To validate previously applied assumptions and further understand the mass transfer process in this system, CFD simulations were performed on a fully submerged rotating drum to determine how the surface-to-bulk mass transfer rate varies with operating conditions.

3.3.1 Governing equations

For an incompressible Newtonian fluid, the governing equations for a transient and unsteady flow are simplified by the mass continuity equation and Navier-Stokes equation [35], which are expressed as:

$$\nabla \cdot U = 0 \tag{3}$$

$$\frac{\partial U}{\partial t} + \nabla \cdot (UU) - \nabla \cdot \upsilon \nabla U = -\nabla \frac{p}{\rho} \tag{4}$$

Where U is the velocity, ν is the kinematic viscosity, ρ is the density, and p is the pressure. For the case of mass transfer into the fluid bulk, the dimensionless concentration of benzoic acid in solution, α, was modeled using a scalar transport equation with turbulent diffusivity contributions:

$$\frac{\partial \alpha}{\partial t} + \nabla \cdot (U\alpha) - \nabla \cdot D_{turb} \nabla \alpha = 0 \quad (5)$$

Where D_{turb} is the diffusion coefficient of benzoic acid in turbulent liquid phase, consisting of the binary diffusivity, D_{AB}, and an enhancement factor dependent on the turbulent eddy viscosity, ν_{turb}, and a turbulent Schmidt number, Sc_{turb}:

$$D_{turb} = D_{AB} + \frac{\nu_{turb}}{Sc_{turb}} \quad (6)$$

3.3.2 Turbulence model

A two-equation SST k-ω model was applied in this work near the surface of the reactor, switching to a k-ε model in the free stream. This approach was adopted in an attempt to better resolve near-wall turbulent effects on mass transfer, whereby the SST k-ω model integrates through the viscous sub-layer down to the wall, and is available with adverse pressure gradients and separating flows [36].

3.3.3 Mesh generation

While the actual experimental system involves an air-water interface, fluid displacement from the reservoir and thin film formation during rotation, our previous compartmental models typically assumed that mass transfer to the reservoir only occurred across the submerged area of the corrugations. With a specific interest on this region, the current simulations were performed for a completely submerged reactor to focus solely on the surface to bulk mass transfer phenomena.

The simulations described here were carried out in OpenFOAM. The corrugated geometries

were first created in an AutoCAD software with physically realistic rounded corners at the apex, after which *snappyHexMesh* was used to generate structured hexahedral meshes of the corrugated reactor (Figure 3.4). The outside domain had dimensions of 150 mm x 150 mm, corresponding to the same width as the reactor tank but twice the height. Considering the concentration boundary layer is much smaller than the velocity boundary layer, localized mesh refinement was introduced within the near-wall region [37]. Drum rotation was achieved using dynamic mesh motion, whereby a sliding boundary was created between the rotational mesh and fixed mesh. Arbitrary mesh interface (AMI) in the OpenFOAM v2.1.0 package allowed the simulation across the disconnected but adjacent mesh domains [38]. A circle with 120 mm diameter surrounding the drum was set to be the AMI boundary, as seen in Figure 3.4.

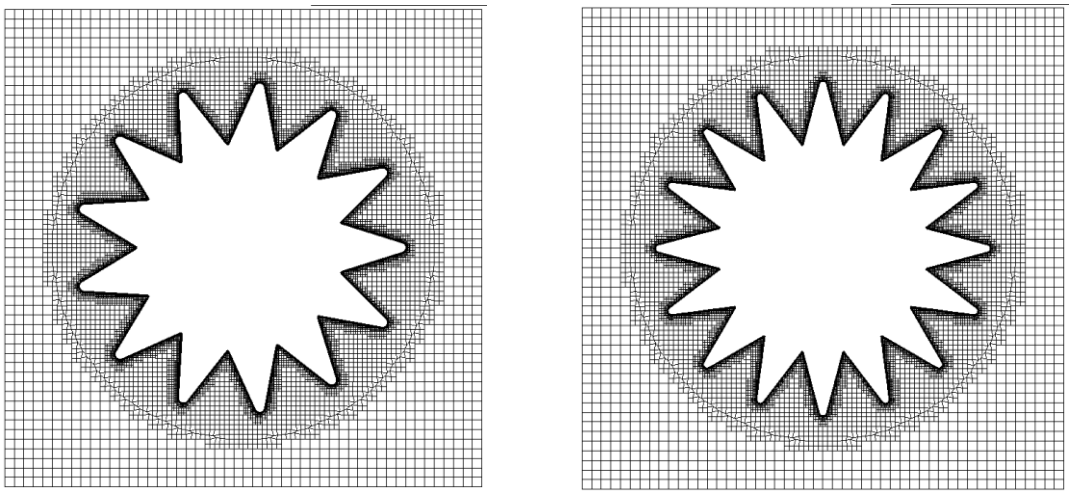

(a) (b)

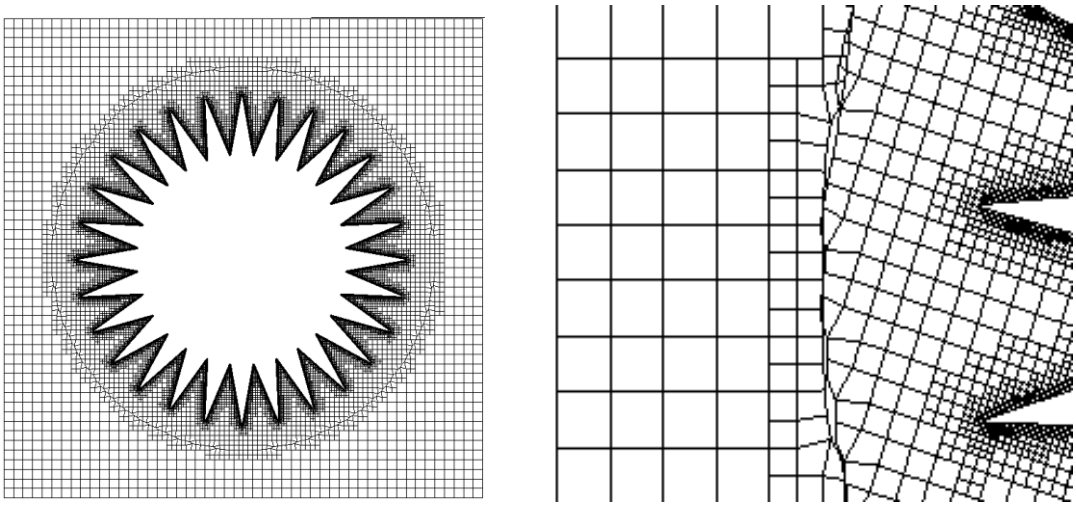

(c) (d)

Figure 3.4 Mesh used in three different angle reactors and rotational interface: (a) 13corrugations (b) 16corrugations (c) 28 corrugations (d) enlargement of rotational interface where AMI is applied.

3.3.4 Boundary conditions

No-slip boundary conditions were applied for the sides and bottom of the external domain, with a free surface on the top. The corrugation walls were also defined as non-slip, with the domain rotated at a specified RPM. Zero-gradient pressure and concentration conditions were applied on all solid boundaries, except the surface of the corrugated reactor where a dimensionless concentration of 1 was applied. Wall functions were applied at solid surfaces for the calculation of turbulent kinetic energy.

3.3.5 Physical properties

Due to the saturation concentration of benzoic acid in water at temperature 20°C being only 2.9 g/L, the kinetic viscosity and density of water were assumed constant during the process,

with values of 1.003×10^{-6} m^2/s [39] and 998.2 kg/m^3. The binary diffusivity of benzoic acid in water, D_{AB}, was set at 1×10^{-9} m^2/s, corresponding to a median point between reported values at infinite dilution, 1.25×10^{-9} m^2/s, and at higher concentrations, 0.75×10^{-9} m^2/s [40].

3.4 Results and discussion

3.4.1 Experimental results

Mass transfer coefficients, which represent the conductance of solids transferred across the solid-liquid interface, are influenced by the dynamic properties of the liquid phase, geometry of the reactor, and characteristics of the solid phase. In this work, the effects of various experimental parameters such as rotational speed, volume of water, and drum configuration on mass transfer coefficients were studied.

3.4.1.1 Effect of rotational speed

The evolution of benzoic acid concentrations under different rotational speeds are shown in Figure 3.5 for the experimental system, illustrating the increased dissolution rate of benzoic acid at higher rotational rates of the drum. The calculated values from Eq.2 fit the experimental data closely, thus the mass transfer coefficient obtained by least-squares regression was deemed reliable. The corresponding volumetric mass transfer coefficient (Figure 3.6) increased by a factor of 2-6 as the rotational rate ranged from 5 to 80 rpm. This was attributed to the increased transfer rate between the corrugated regions and bulk solution due to turbulence near the corrugated drum as the rotational rate increased and greater local

concentration. Since the drum was partially submerged in the liquid reservoir, the liquid film would be carried by the corrugations during the rotation. The liquid film formed on the upper surface of the drum was also influenced by the rotational rate. Low velocities resulted in the liquid film dropping due to the acting gravitational force, while at high velocities the liquid film was maintained in continuous contact with the surface of the drum thus increasing apparent mass transfer.

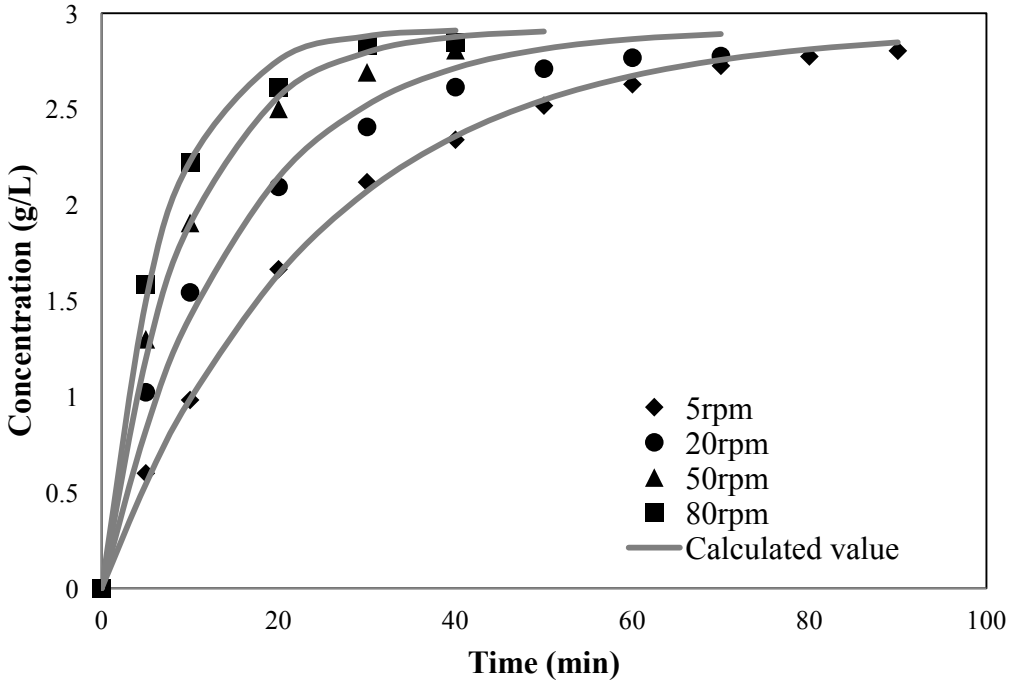

Figure 3.5 Effect of rotational speed on benzoic acid concentration for the 28 corrugations reactor at 1.6 L volume

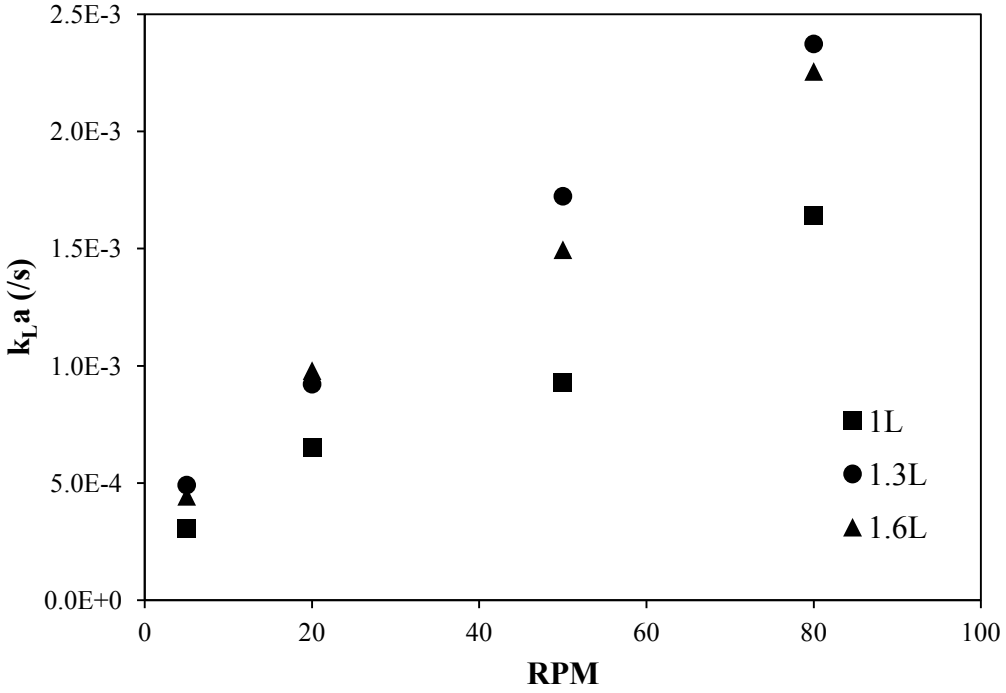

(a) 13 corrugations

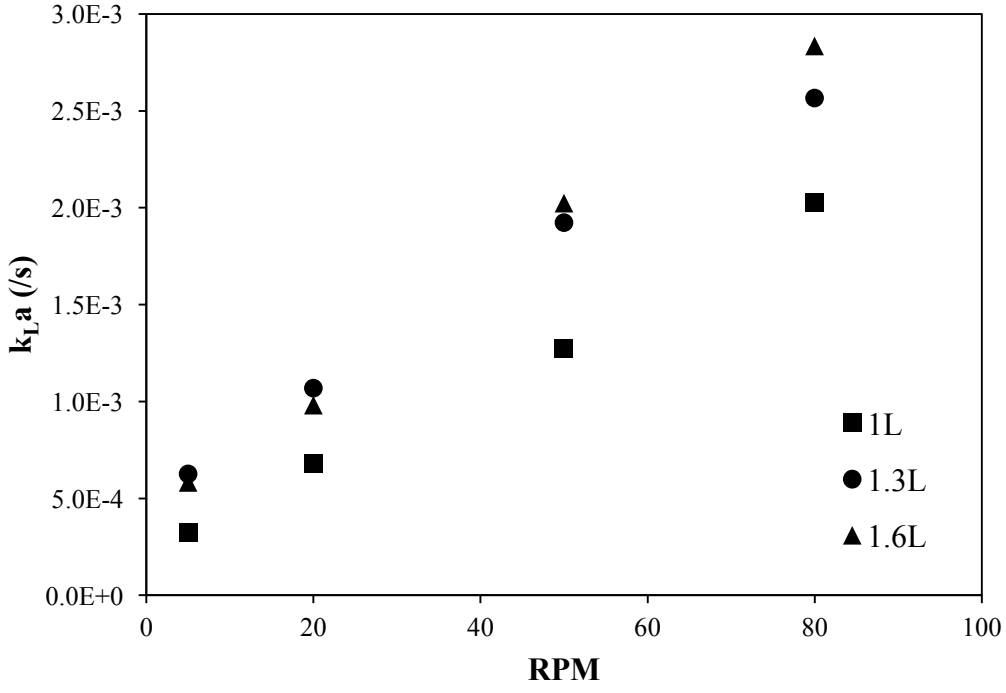

(b) 16 corrugations

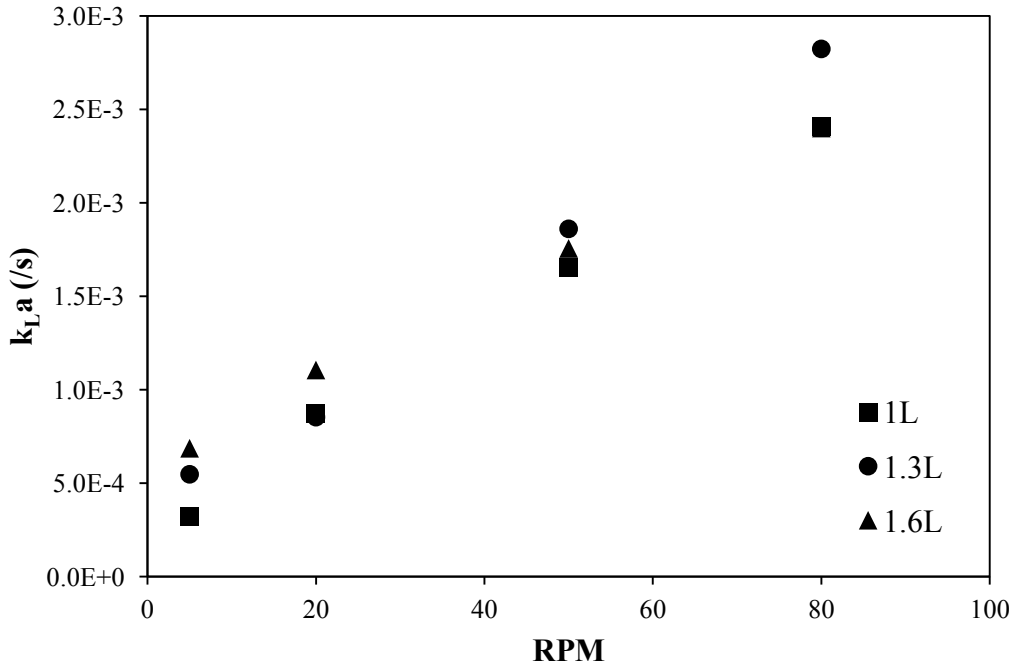

(c) 28 corrugations

Figure 3.6 Effect of rotational speed on mass transfer coefficients for 13 corrugations (a), 16 corrugations (b) and 28 corrugations (c) reactors

3.4.1.2 Effect of water volume

The volume of water within the reservoir directly affected the submerged surface area of the drum and the amount of water that was carried to the upper section of the drum by the corrugations. The volumetric mass transfer coefficients obtained using volumes of water ranging from 1 L to 1.6 L and their corresponding submerged areas are shown in Figure 3.7 and Table 3.1 for three reactor configurations. Based the obtained data, the volumetric mass transfer coefficients at the 1 L volume were found to be much lower than at other volumes for the various reactors. This was thought to be due to the smallest surface area of the

corrugations being submerged in the water at this volume, and because mass transfer mainly occurred from the submerged surface of the drum to the bulk solution. The relative variation in mass transfer rates for the 1 L to 1.3 L increase was far more than that observed from 1.3 L to 1.6 L. This was thought to be caused by the relative differences of submerged area of the drums. The variation of submerged areas between 1 L and 1.3 L were larger than those observed between the 1.3 L and 1.6 L water volume for all drums. However, the mass transfer rate at the 1.6 L volume, which corresponded to the largest submerged area, were less than those observed at the 1.3 L water volume. This indicated that the mass transfer rates were influenced by both the submerged area of the drums as well as the quantity of water circulating within the corrugations. For the 1.3 L and 1.6 L water volumes, a larger surface area of the drum was submerged in the liquid, and the angle between the water surface and the drum allowed for a small quantity of water to circulate within the corrugations. More contact between the coated surface and liquid film present above the reservoir was expected to lead to faster rates of mass transfer. However, under these circumstances, more bubbles would be formed between corrugations when the drum rotated out of the water at a higher water level. This would reduce the mass transfer between the liquid film and coated area at the upper section of the drum. Therefore, the mass transfer rate was thought to be dictated mainly by the submerged surface area, but was also influenced by the water carried within corrugations and bubbles.

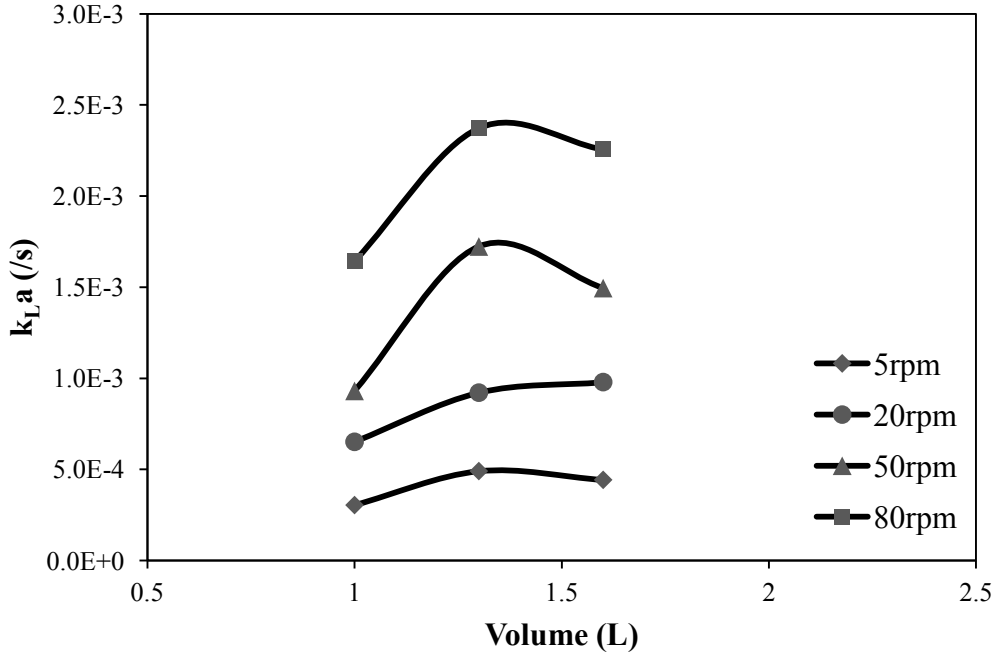

(a) 13 corrugations

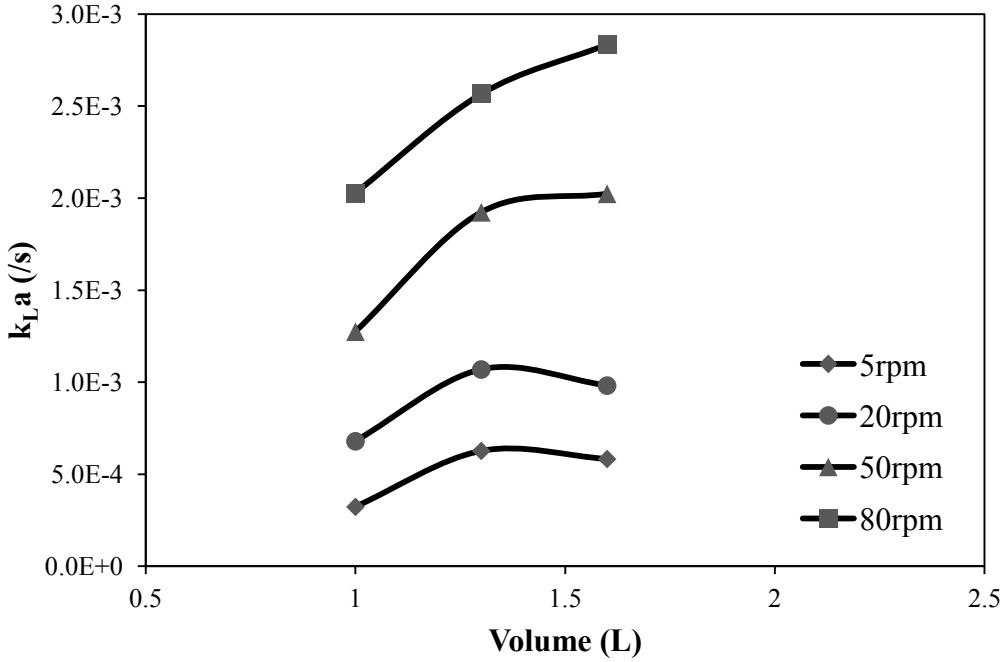

(b) 16 corrugations

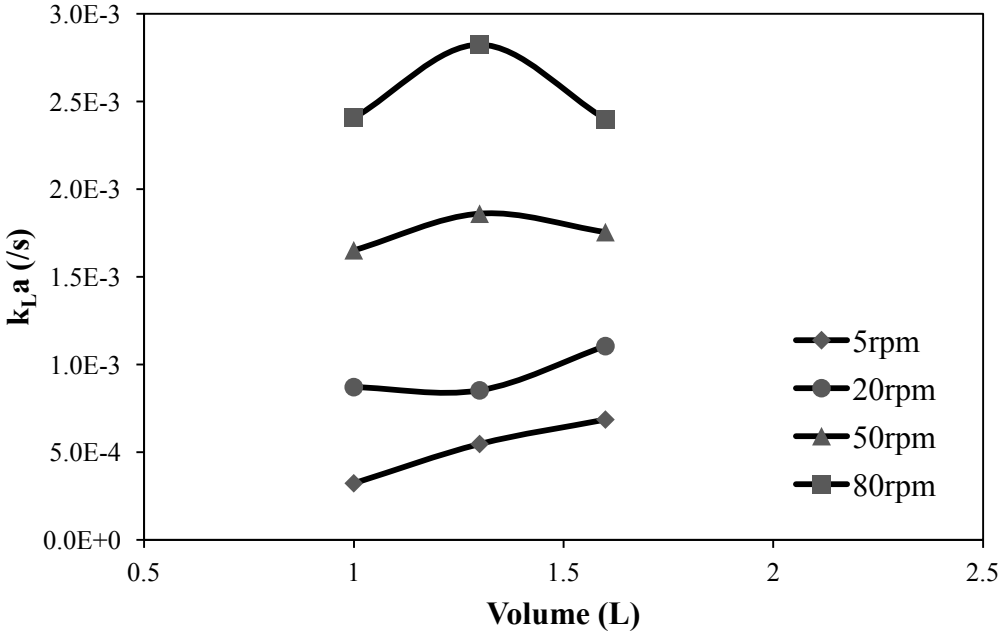

(c) 28 corrugations

Figure 3.7 Effect of water volume on volumetric mass transfer coefficients for 13 corrugations (a), 16 corrugations (b) and 28 corrugations (c) reactors

3.4.1.3 Effect of various configurations

Each experiment was performed with three different drums having 13, 16, and 28 corrugations, respectively. The mass transfer coefficients using the various drums at four rotational speeds are shown in Figure 3.8, where the k_L was an average mass transfer coefficient under different water volume conditions. Based on these results, the drum with 28 corrugations had a lower mass transfer coefficient than other drums at each rotational speed. Though the drum with 28 corrugations had a higher mass transfer rate (Figure 3.9), the larger submerged surface area resulted in a lower k_L. The difference in mass transfer coefficients

between the drum with 28 corrugations and others increased with increasing rotational speed. This was due to the reduction of solid-liquid mass transferred in the small angle between two corrugations. This small space impeded the transfer of the high concentration solution near the surface of the corrugation to the bulk solution. In the 16 and 13 corrugation reactors, however, there were wider spaces between corrugations which enabled liquid exchange between the bulk liquid and the surface of the drum.

Another important phenomenon is the formation of bubbles between corrugations when the drum rotated out of the water. At higher rotational speed, and at smaller corrugation angles, larger amounts of bubbles were generated. Thus the mass transfer rate at the upper side of the reactor decreased.

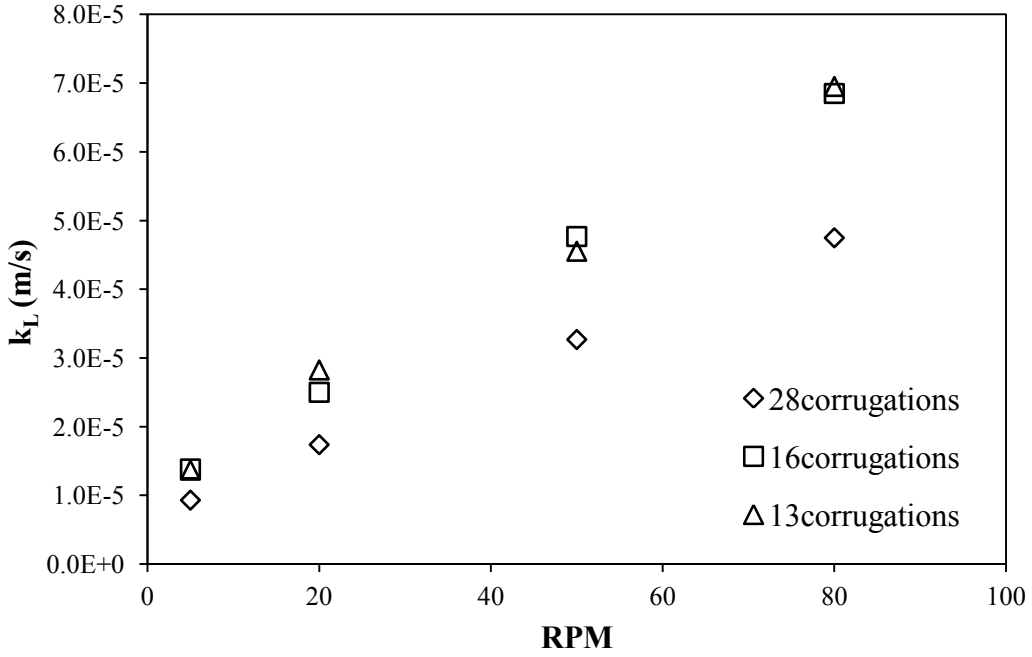

Figure 3.8 Effect of number of corrugations on the mass transfer coefficient at different rotational speeds

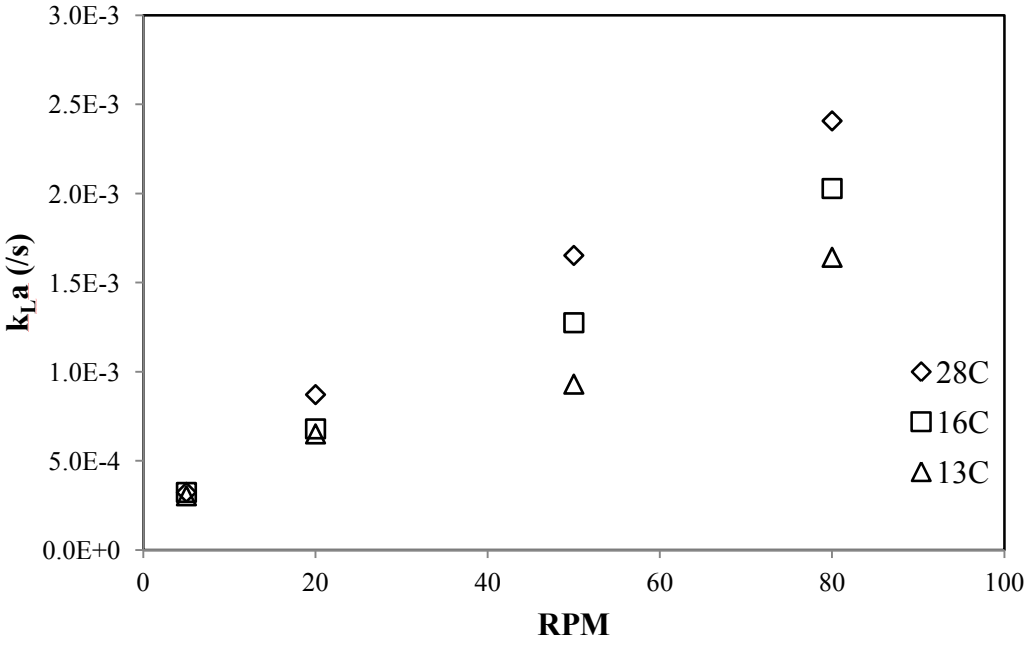

Figure 3.9 Effect of number of corrugations on the volumetric mass transfer coefficient at 1 L water volume

3.4.1.4 Effect of bubble formation

As shown in Figure 3.10, bubbles often formed on the surface of the drum when it was not submerged. At high rotational speed, there was insufficient time for the bubbles to collapse and drain from the water, and they therefore rotated with the drum throughout the process. At increasing rotational speed, the size of the bubbles decreased, but their number increased. At lower rotational rates, the bubbles had sufficient time to burst before reaching the peak of the rotation. No bubbles were observed at 5 rpm in these experiments.

The volume of water in the reactor also affected the bubble formation. The drums with larger percentages of their surface areas immersed in water enabled the formation of more bubbles. As previously mentioned, in such cases the liquid film was more likely to be carried up to the atmosphere, increasing the chance for bubbles to be generated.

Additionally, bubble formation was influenced by the configuration of reactors. As the drums rotated, the air between smaller corrugation angles did not drain as easily due to their buoyancy.

The impact of the bubbles on solid-liquid mass transfer was therefore a complex function of the rotational speed, volume of water, and drum configuration, as well as of the liquid film thickness on the surface of the drum.

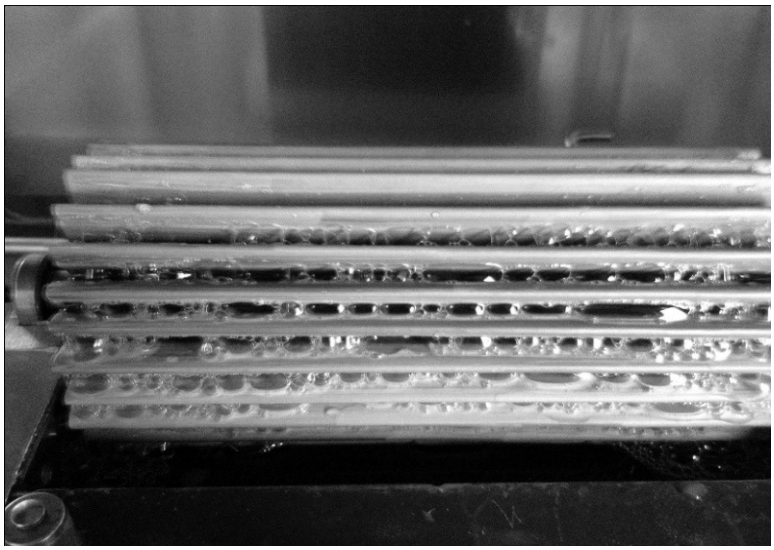

Figure 3.10 Bubble formation on the surface of reactor

3.4.2 Modeling results

While in the experimental system the mass transfer occurred between the submerged surface and bulk solution as well as between the coated surface and liquid thin film formed at the upper drum, the previous work assumed that the mass transfer only occurred across the submerged surface of the corrugations. To further explore this issue, a fully submerged corrugated reactor was modeled. To validate the flat-plate correlations used to simulate bulk to surface mass transfer in the previous work, the velocity and concentration fields of corrugated reactors were simulated and mass transfer coefficients were compared with the flat-plate correlations.

3.4.2.1 Velocity field

The velocity of the flow region in all reactors at a rotational speed of 80 rpm is shown in Figure 3.11. From the simulation results, the liquid between the corrugations was observed to

flow rotationally with the drum at a similar speed, while the liquid closer to the tank walls flowed more slowly. For different reactors at the same rotational speed, the same velocity patterns and magnitude were observed.

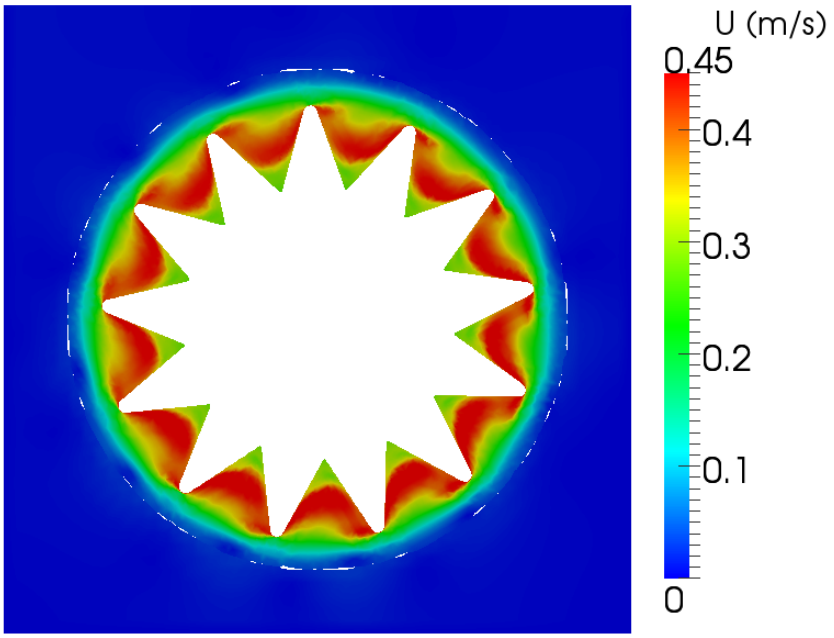

(a) 13 corrugations

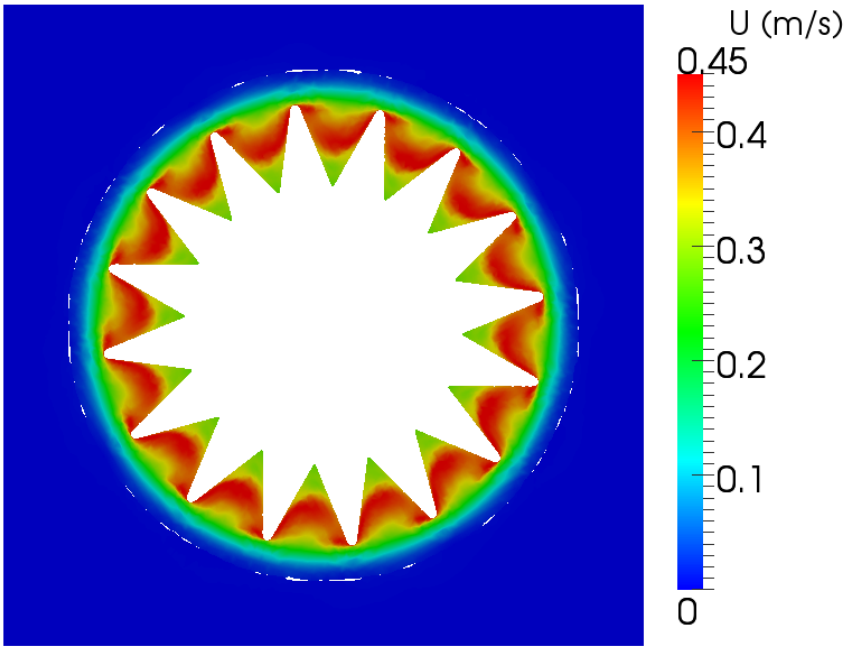

(b) 16 corrugations

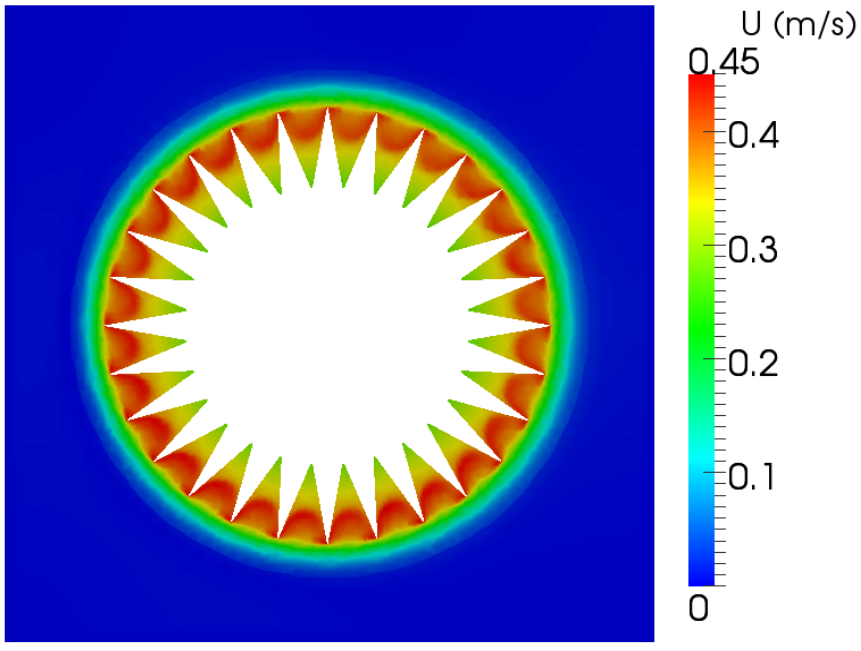

(c) 28 corrugations

Figure 3.11 Magnitude of velocity for the 13 corrugations (a), 16 corrugations (b) and 28 corrugations (c) reactors operated at 80rpm

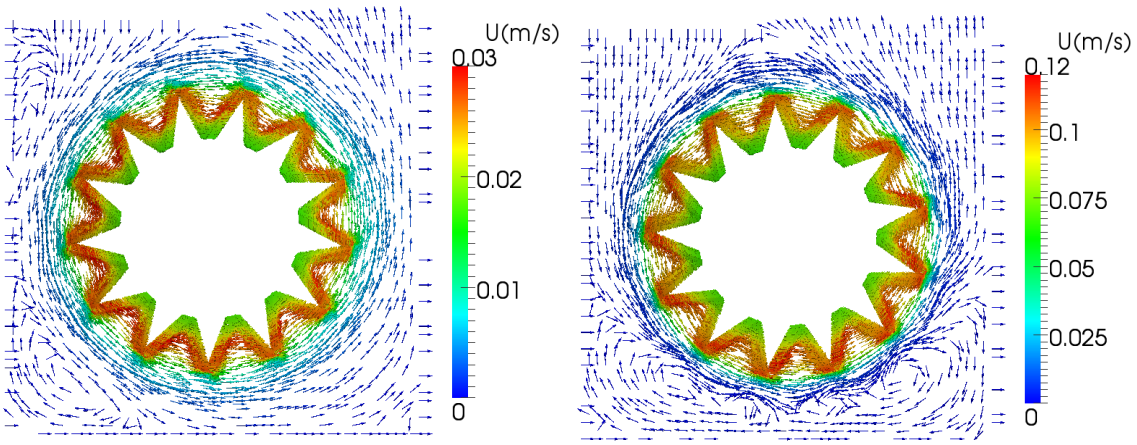

(a) 5 rpm (b) 20 rpm

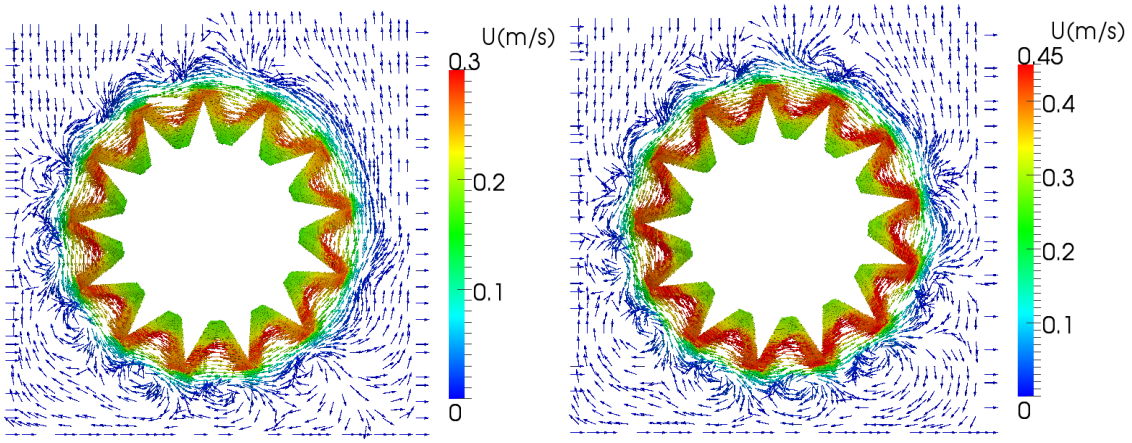

(c) 50 rpm (d) 80 rpm

Figure 3.12 Velocity vectors for the 13 corrugations reactor at different rpm

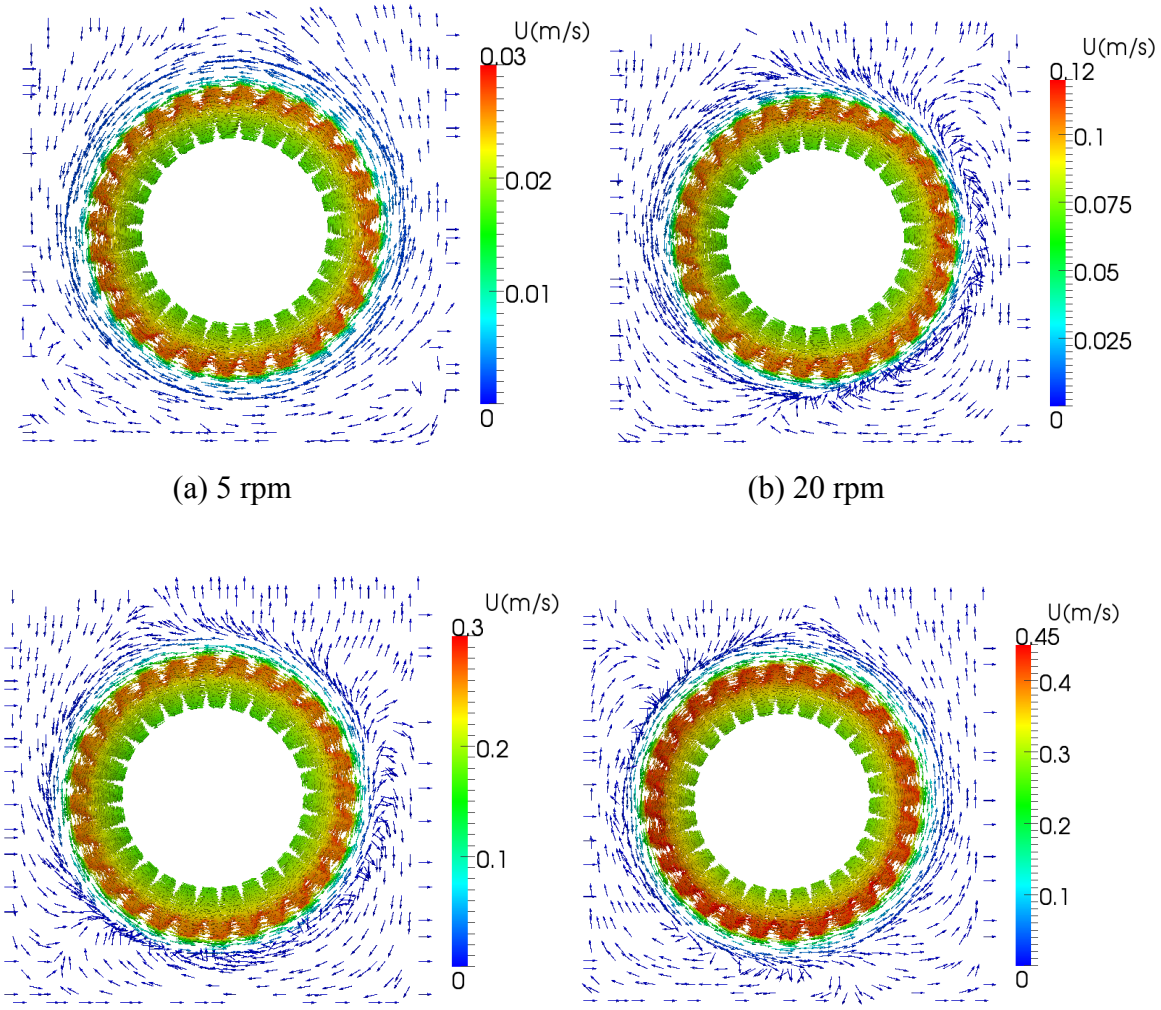

(a) 5 rpm (b) 20 rpm

(c) 50 rpm (d) 80 rpm

Figure 3.13 Velocity vectors for the 28 corrugations reactor at different rpm

The simulations predicted distinct vortex zones for different corrugated reactors at various rotational speeds. Figures 3.12-3.13 show the velocity vectors of the entire simulated region for all reactors and rotational speeds. With increasing rotational speeds, the vortices occurred not only at the corners of the reservoir but also near the moving drum. As the rotational speed increased, the number of vortices increased as well. These characteristics existed for all reactors but were particularly apparent for the 13 corrugations reactor. This was thought

to be due to the larger angles between corrugations being more likely to generate small vortices around the drum. At the same rotational speed, the flow was less chaotic for the 28 corrugations reactor than the 13 corrugations reactor.

3.4.2.2 Concentration field

The dimensionless concentration patterns of benzoic acid for the various reactors are given in Figure 3.14. The dimensionless concentration of benzoic acid at the surface of the drums was set as 1, corresponding to the saturated concentration of benzoic acid (2.9 g/L). Some mass transfer phenomena existed in the simulation, namely: mass transfer from the surface of corrugation to the volume occurred between every two corrugations, and mass transfer occurred across the boundary layer that formed between spinning corrugated reactor and bulk solution. From the results observed, a high concentration of benzoic acid was found at the bottom of the triangular zone between two corrugations. As the drum moved counter-clockwise, the rate of dissolution of benzoic acid at the right side of each corrugation was faster than that of the left side. The benzoic acid transferred from the surface to the volume between every corrugation, which quickly led to a high concentration zone within the rotational reactor. The mass of benzoic acid accumulated at the fold region, however, slowly transported from the rotational region to the bulk solution, especially for the 28 corrugations. This was due to the little movement perpendicular to the rotational direction in 28 corrugations. Benzoic acid deposited at the smaller corrugation volume hardly transferred

across the boundary layer formed by the spinning reactor to the bulk solution. The concentration of bulk solution in the 28 corrugation reactor was lower than that observed in the others. This difficulty was overcome by increasing the angle between two corrugations. However, in the real experimental system, the fluid in the corrugation was effectively drained each time it left the free surface, so the mass transfer limitations between the corrugation volume and the bulk solution did not exist.

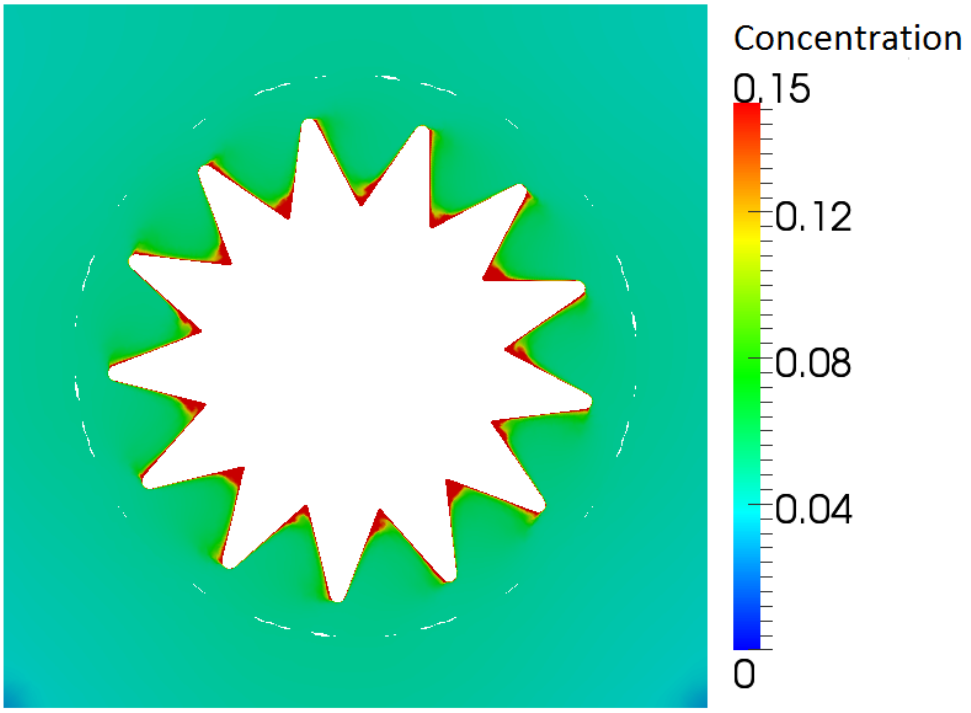

(a) 13 corrugations

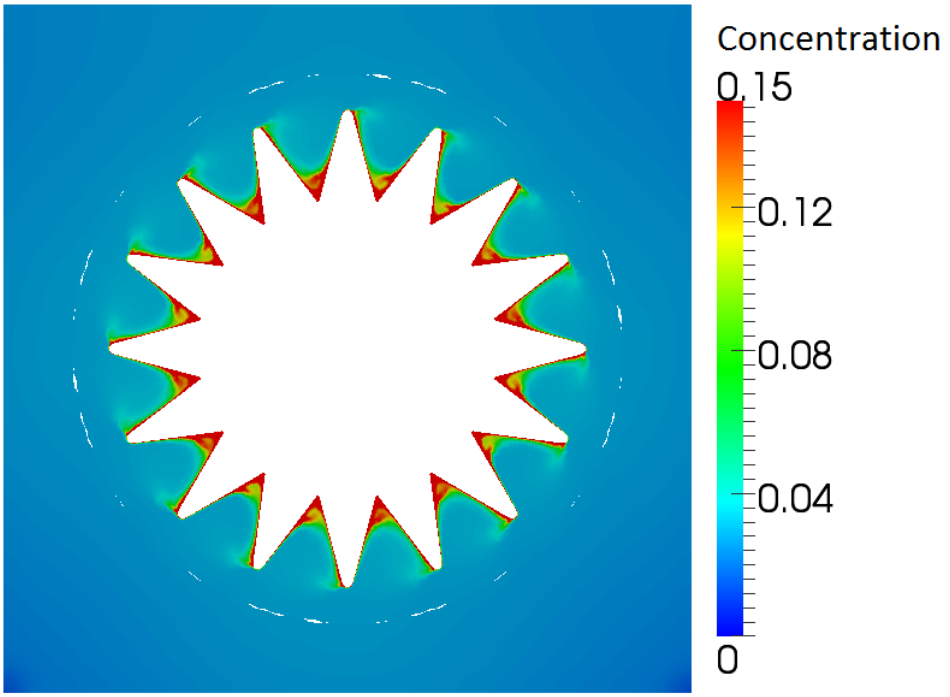

(b) 16 corrugations

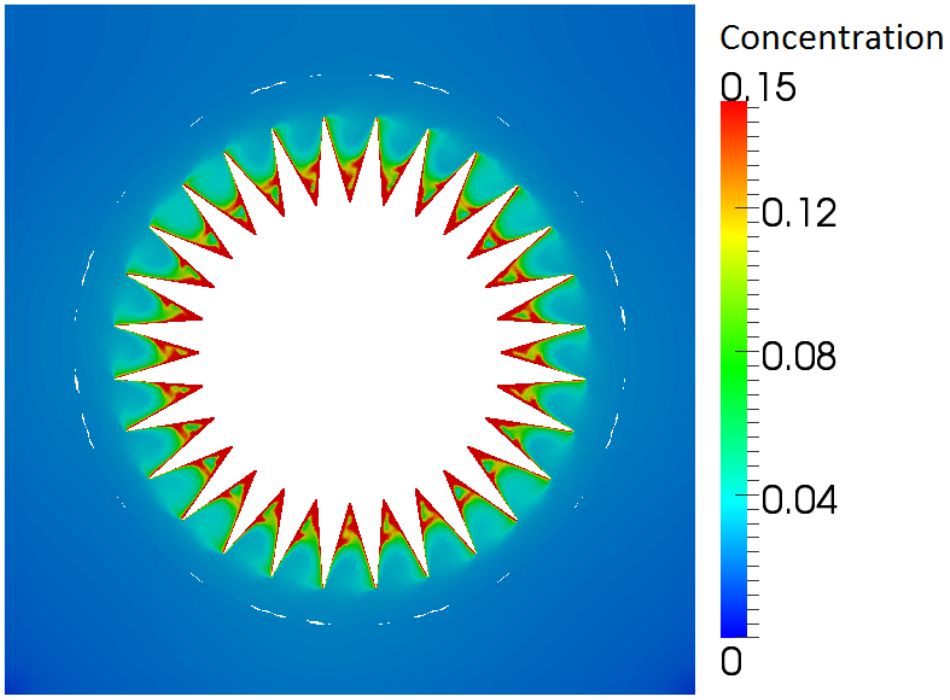

(c) 28 corrugations

Figure 3.14 Mass fraction of benzoic acid at 100 seconds and 5 rpm for the different reactors

3.4.2.3 Mass transfer coefficients

The experimental and simulated mass transfer coefficients for the three reactors at various rotational speeds are shown in Figure 3.15. The simulation results were found to be lower than the experimental results, and varied more greatly with increasing rotational speed. This was due to the mass transfer limitation between the corrugation volume and the bulk solution which existed in the simulation. This mass transfer limitation did not occur in the experimental system, since the fluid in the corrugation effectively drained each time it left the free surface. This factor is likely responsible for the underestimated mass transfer rates compared to the experimental results.

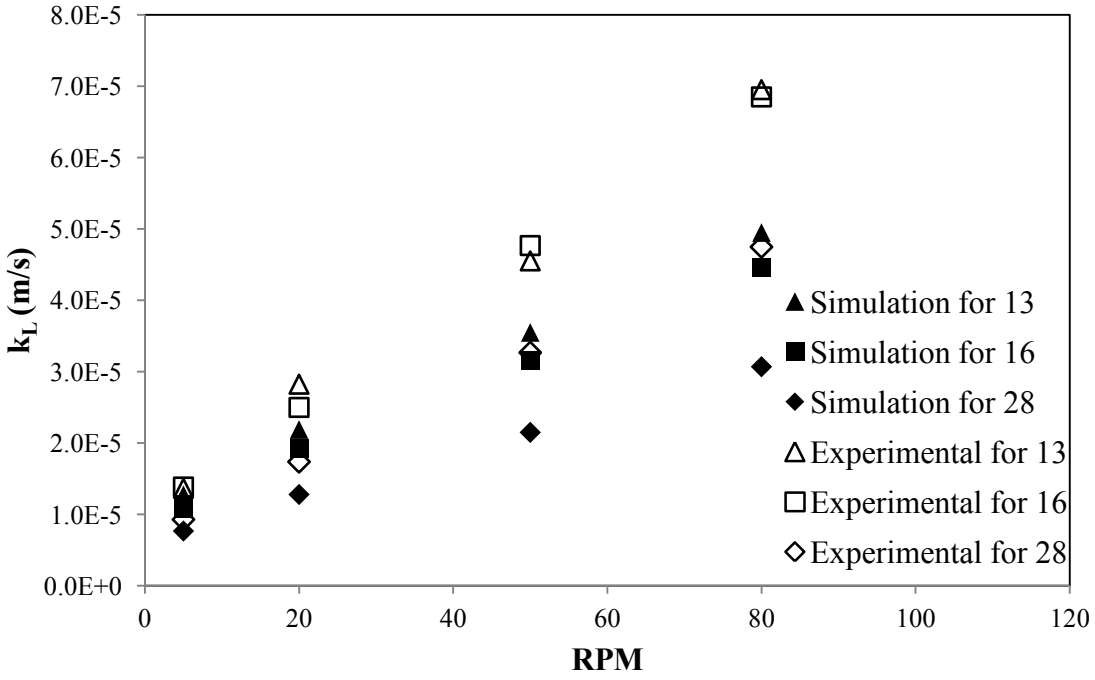

Figure 3.15 Comparison of the mass transfer coefficients obtained from CFD simulations and those obtained experimentally for the three reactors.

3.4.2.4 Local mass transfer coefficients

The weighting factors of mass transfer coefficients along the drum surface are shown in Figure 3.16. The configuration of the drums affected the peak locations for mass transfer, which were observed to be at the middle point or at the extremities of the corrugations. For the 13 corrugations reactor, the highest local mass transfer coefficient was found at the middle point of the corrugation, as the large space between the corrugations allowed for good mixing. This result indicated that the liquid was sufficiently mixed around the large angle corrugations. For the 28 corrugations reactor, the small space between adjacent corrugations limited the transfer of liquid from the reactor walls to the bulk liquid, and the highest rate of mass transfer was therefore observed at the extremity of the corrugations.

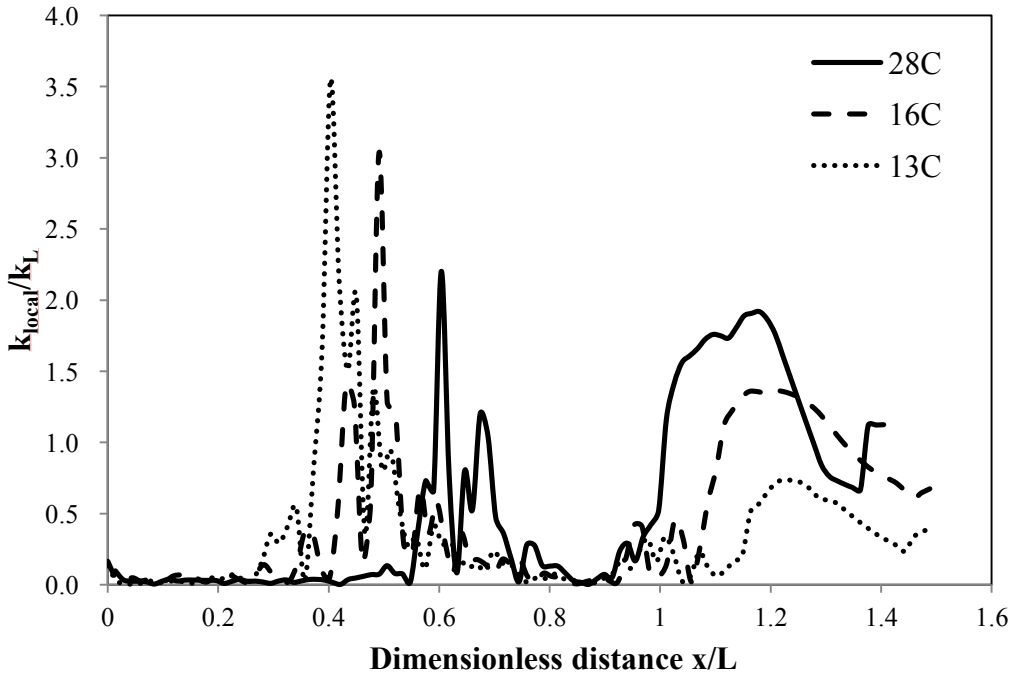

Figure 3.16 Local mass transfer coefficients along the drum surface

3.4.3 Correlation equations of mass transfer

The correlation equations of mass transfer are written in the form of:

$$Sh = aRe^{b}Sc^{c} \tag{7}$$

where the Sherwood number, Reynolds number and Schmidt number are respectively expressed as:

$$Re = \frac{\omega r d}{\nu} \tag{8}$$

$$Sh = \frac{k_L d}{D_{AB}} \tag{9}$$

$$Sc = \frac{\nu}{D_{AB}} \tag{10}$$

The experimental and simulation data and correlations of *Sh* with various *Re* in three corrugated reactors are shown in logarithmic coordinates in Figure 3.17. The results obtained indicate that the Sherwood number of the corrugated reactor is much greater than that of flat-plate reactors. Therefore, the flat-plate mass transfer correlation used in this corrugated system does not represent the system accurately. The correlation equations with fitted coefficients for each reactor, with rotational speeds in the range of 2500< Re<50000, are shown in equation 11-13 for the simulation and in equations 14-16 for the experiment, respectively:

Simulation:

$$\text{13C:}\quad Sh = 2.7933Re^{0.4800}Sc^{0.33} \tag{11}$$

$$\text{16C:}\quad Sh = 2.0505Re^{0.4990}Sc^{0.33} \tag{12}$$

$$28C: \quad Sh = 1.5243Re^{0.4904}Sc^{0.33} \tag{13}$$

Experiment:

$$13C: \quad Sh = 1.5037Re^{0.5686}Sc^{0.33} \tag{14}$$

$$16C: \quad Sh = 1.4076Re^{0.5735}Sc^{0.33} \tag{15}$$

$$28C: \quad Sh = 0.8828Re^{0.5829}Sc^{0.33} \tag{16}$$

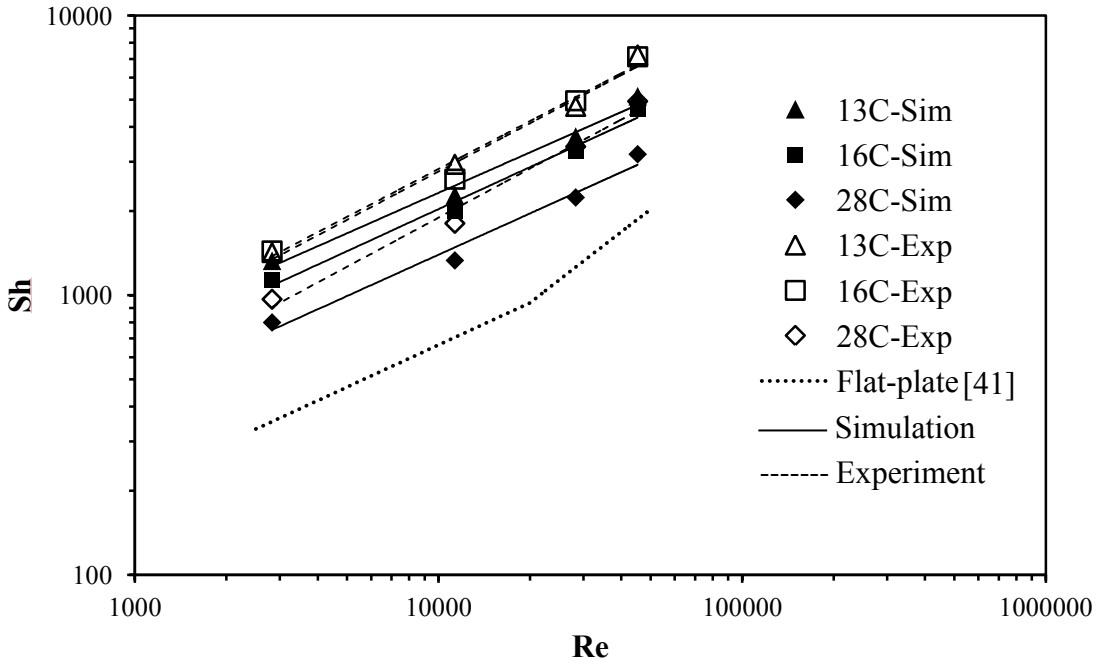

Figure 3.17 Sherwood and Reynolds numbers correlations for the different reactors

3.5 Conclusions

In this work, experiments and simulations were carried out in order to analyze mass transfer processes in corrugated photocatalytic reactors. The mass transfer coefficients for photocatalytic reactors with 13, 16, and 28 corrugations were evaluated using the benzoic

acid dissolution method at rotational speeds ranging from 5 rpm to 80 rpm, and water volumes ranging from 1 L to 1.6 L.

According to the experimental results, the mass transfer rates increase with increasing drum rotational speeds as the result of the generation of eddies in turbulent flow and the formation of a liquid film on the upper side of the drum. Additionally, a significant effect of water volume on mass transfer was observed when the drum was immersed at a low water level due to the small submerged surface area of the corrugations. It was also found that as the number of corrugations of the drum increased, the mass transfer coefficients in the reactors decreased. The latter was a result of the small angle between corrugations which limited the transport of benzoic acid from the surface of the drum to the bulk solution. Consequently, the drum with 28 corrugations, which had a higher mass transfer rate, had a lower mass transfer coefficient than the other reactors. The formation of bubbles was another factor that influenced the mass transfer processes. The bubble formation in the system was also thought to be related to the rotational speed, the volume of water, and the drum configuration.

The CFD simulations were used to predict the velocity and concentration fields within the reactors, which represented the fluid flow conditions and solid–liquid transport processes. The drum with 13 corrugations had more vortex regions than the others. The mass transfer limitations between the corrugation volume and bulk solution in the simulation caused lower mass transfer coefficients than in the experiments. The correlation obtained indicated that the flat-plate mass transfer correlation could not be used in the corrugated system.

The mass transport phenomena in corrugated photocatalytic reactors studied in this work provide a better understanding of general transport processes and should facilitate future reactor optimization.

3.6 References

[1] M.R. Hoffmann, S.T. Martin, W. Choi, D.W. Bahnemann, Environmental applications of semiconductor photocatalysis, Chemical Reviews, 95 (1995) 69-96.

[2] M. Anpo, Utilization of TiO_2 photocatalysts in green chemistry, Pure and applied chemistry, 72 (2000) 1265-1270.

[3] C. McCullagh, N. Skillen, M. Adams, P.K.J. Robertson, Photocatalytic reactors for environmental remediation: a review, Journal of Chemical Technology & Biotechnology, 86 (2011) 1002-1017.

[4] P.G. Hoertz, D. Magnus-Aryitey, V. Gupta, C. Norton, S. Doorn, T. Ennis, Photocatalytic and radiocatalytic nanomaterials for the degradation of organicspecies, Radiation Physics and Chemistry, 84 (2013) 51-58.

[5] S. Shenawi-Khalil, V. Uvarov, S. Fronton, I. Popov, Y. Sasson, A novel heterojunction BiOBr/bismuth oxyhydrate photocatalyst with highly enhanced visible light photocatalytic properties, Journal of Physical Chemistry C, 116 (2012) 11004-11012.

[6] C. Shifu, Z. Sujuan, L. Wei, Z. Wei, Study on the photocatalytic activity of p-n junction photocatalyst Cu_2O/TiO_2, Journal of Nanoscience and Nanotechnology, 9 (2009) 4397-4403.

[7] C.H. Lin, J.W. Lee, C.Y. Chang, Y.J. Chang, Y.C. Lee, M.Y. Hwa, Novel TiO_2 thin films/glass fiber photocatalytic reactors in the removal of bioaerosols, Surface and Coatings Technology, 205 (2010) S341-S344.

[8] D. Zhang, L. Zhang, H. Li, Influence of reactor types on photocatalytic oxidation performance of organic wastewater in slurry reactors, Huaxue Fanying Gongcheng Yu Gongyi/Chemical Reaction Engineering and Technology, 22 (2006) 7-13.

[9] C.M. Ling, A.R. Mohamed, S. Bhatia, Performance of photocatalytic reactors using immobilized TiO_2 film for the degradation of phenol and methylene blue dye present in water stream, Chemosphere, 57 (2004) 547-554.

[10] G. Li Puma, P.L. Yue, Modelling and design of thin-film slurry photocatalytic reactors for water purification, Chemical Engineering Science, 58 (2003) 2269-2281.

[11] D.M. Lee, H.J. Yun, S. Yu, S.J. Yun, S.Y. Lee, S.H. Kang, J. Yi, Design of an efficient photocatalytic reactor for the decomposition of gaseous organic contaminants in air, Chemical Engineering Journal, 187 (2012) 203-209.

[12] G.E. Imoberdorf, A.E. Cassano, H.A. Irazoqui, O.M. Alfano, Optimal design and modeling of annular photocatalytic wall reactors, Catalysis Today, 129 (2007) 118-126.

[13] L. Zhang, W. Anderson, Z. Zhang, Development and modeling of a rotating disc photocatalytic reactor for wastewater treatment, Chemical Engineering Journal, 121 (2006) 125-134.

[14] D. Chen, F. Li, A.K. Ray, External and internal mass transfer effect on photocatalytic

degradation, Catalysis Today, 66 (2001) 475-485.

[15] D. Chen, F. Li, A.K. Ray, Effect of mass transfer and catalyst layer thickness on photocatalytic reaction, AIChE Journal, 46 (2000) 1034-1045.

[16] M.d.l.M. Ballari, O.M. Alfano, A.E. Cassano, Mass transfer limitations in slurry photocatalytic reactors: Experimental validation, Chemical Engineering Science, 65 (2010) 4931-4942.

[17] D.D. Dionysiou, M.T. Suidan, I. Baudin, J.M. Laîné, Oxidation of organic contaminants in a rotating disk photocatalytic reactor: Reaction kinetics in the liquid phase and the role of mass transfer based on the dimensionless Damköhler number, Applied Catalysis B: Environmental, 38 (2002) 1-16.

[18] T.A. McMurray, J.A. Byrne, P.S.M. Dunlop, J.G.M. Winkelman, B.R. Eggins, E.T. McAdams, Intrinsic kinetics of photocatalytic oxidation of formic and oxalic acid on immobilised TiO_2 films, Applied Catalysis A: General, 262 (2004) 105-110.

[19] J. Palau, J.M. Penya-Roja, C. Gabaldón, F. Javier Álvarez-Hornos, F. Sempere, V. Martínez-Soria, UV photocatalytic oxidation of paint solvent compounds in air using an annular TiO_2-supported reactor, Journal of Chemical Technology and Biotechnology, 86 (2011) 273-281.

[20] G. Vincent, E. Schaer, P.M. Marquaire, O. Zahraa, CFD modelling of an annular reactor, application to the photocatalytic degradation of acetone, Process Safety and Environmental Protection, 89 (2011) 35-40.

[21] T.H. Lim, S.D. Kim, Photocatalytic degradation of trichloroethylene (TCE) over TiO_2/silica gel in a circulating fluidized bed (CFB) photoreactor, Chemical Engineering and Processing: Process Intensification, 44 (2005) 327-334.

[22] A.A. Donaldson, Z. Zhang, UV absorption by TiO_2 films in photocatalytic reactors: Effect of fold curvature, AIChE Journal, 58 (2012) 1578-1587.

[23] H. Shang, Z. Zhang, W.A. Anderson, Nonuniform radiation modeling of a corrugated plate photocatalytic reactor, AIChE Journal, 51 (2005) 2024-2033.

[24] Z.J. Zhang, W.A. Anderson, M. Moo-Young, An Engineering Model for the Scale-up and Design of Photocatalytic Reactors, International Journal of Chemical Reactor Engineering, 1 (2003) 57.

[25] Z. Zhang, W.A. Anderson, M. Moo-Young, Modeling of corrugated plate photocatalytic reactors and experimental validation, Chemical Engineering Science, 58 (2003) 911-914.

[26] Z. Zhang, Analysis of a corrugated-plate photocatalytic reactor, Ph.D. Thesis, University of Waterloo, Canada, 1999.

[27] Z. Zhang, W. Anderson, M. Mooyoung, Experimental analysis of a corrugated plate photocatalytic reactor, Chemical Engineering Journal, 99 (2004) 145-152.

[28] Z. Zhang, W.A. Anderson, M. Moo-Young, Rigorous Modeling of UV Absorption by TiO_2 Films in a Photocatalytic Reactor, AIChE Journal, 46 (2000) 1461-1470.

[29] D. Adam, Z. Zisheng, M.R. Abdelaal, Coupled Transport Phenomena in Corrugated Photocatalytic Reactors, Chinese Journal of Chemical Engineering, 19 (2011) 763-772.

[30] S.M. Meunier, J. Gamage, Z. Duvnjak, Z. Zhang, Design and Characterization of a Novel Rotating Corrugated Drum Reactor for Wastewater Treatment, International Journal of Photoenergy, 2010 (2010) 1-10.

[31] M. Turkyilmazoglu, Exact solutions for the incompressible viscous fluid of a porous rotating disk flow, International Journal of Non-Linear Mechanics, 44 (2009) 352-357.

[32] J. Zhang, W. Fu, J. Xi, H. He, S. Zhao, H. Lu, Z. Ji, N-doped rutile TiO_2 nano-rods show tunable photocatalytic selectivity, Journal of Alloys and Compounds, 575 (2013) 40-47.

[33] P. Harriott, R. Hamilton, Solid-liquid mass transfer in turbulent pipe flow, Chemical Engineering Science, 20 (1965) 1073-1078.

[34] W. Hess, Kirk-Othmer encyclopedia of chemical technology, John Wiley & Sons Ltd., New York, 1995.

[35] H.K. Versteeg, W. Malalasekera, An Introduction to computational Fluids Dynamics, 2nd Edition Pearson, England, 2007.

[36] B. Andersson, R. Andersson, L. Hakansson, M. Mortensen, R. Sudiyo, B V. Wachem, Computational Fluid Dynamics for Engineers. Cambridge, 2012.

[37] J. Esteban Duran, F. Taghipour, M. Mohseni, CFD modeling of mass transfer in annular reactors, International Journal of Heat and Mass Transfer, 52 (2009) 5390-5401.

[38] OpenCFD Ltd. OpenFOAM® v2.1.0: Arbitrary Mesh Interface (AMI), Available at http://www.openfoam.org/version2.1.0/ami.php, 2011.

[39] J. Keslin, Viscosity of Liquid Water in the Range—8 C to 150 C, J. Phys. Chem. Ref.

Data, 7 (1978).

[40] S. Irandoust, B. Andersson, Concentration-dependent diffusivity of benzoic acid in water and its influence on the liquid–solid mass transfer, The Canadian Journal of Chemical Engineering, 64 (1986) 954-959.

[41] Jules Thibault, Advanced Transport Phenomena, University of Ottawa, Canada, 2010.

CHAPTER 4

Conclusions and Future Work

4.1 Conclusions

Though the researches in the application of photocatalysis for wastewater treatment have grown exponentially, photocatalytic reactions also create their own problems that mass transfer limitations significantly influence the degradation rate. To further promote the development of photocatalysis for wastewater treatment, mass transfer processes existing in photocatalytic reactions and reactors must be studied in order to understand and optimize the process, and to improve the efficiency of pollutants degradation.

In this work, the analysis of mass transfer processes in a novel corrugated drum photocatalytic system was presented through experiments and simulations. The mass transfer coefficients were measured at rotational speeds ranging from 5 rpm to 80 rpm and reactor water volume from 1 L to 1.6 L for reactor designs with 13, 16, and 28 corrugations, respectively. The results indicated that the mass transfer rates increased with increasing rotational speed of the drum. The water volume had significant effect on mass transfer rate when the drum was immersed to cover 20% of its surface area. The drum with 28

corrugations had better mixing condition compared to the other drums due to the large submerged surface area of the corrugations but a lower mass transfer coefficient since the small angle between corrugations, which caused the solution to be transported more difficultly from the surface of the drum to the bulk. Bubble formation on the surface of the drum also affected the mass transfer rate. Additionally, the simulations were used to predict the velocity and concentration patterns within the reactors. It was found that the drum with 13 corrugations had more vortex regions than the others. The mass transfer limitations between the corrugation volume and bulk solution in the simulation caused lower mass transfer coefficients than in the experiments.

4.2 Future work

The performance of other turbulent models is recommended to simulate the velocity field within reactors, and the comparison of these turbulent models is also necessary. Since the simulation in this work based on single phase flow, which is a simplification from the experiments, two phase flow simulations should be investigated in the future.

The effect of drums prepared with different corrugation angles should also be simulated and compared in order to optimize this novel photocatalytic reactor.

APPENDIX A

Turbulence model for simulations

The shear-stress transport (SST) k-ω turbulence model is a hybrid model combining the Wilcox k-ω and the k-ε models by using a blending function. It utilizes the Wilcox k-ω model in the near-wall region and a standard k-ε model in the fully turbulent region far from the wall. This model is well suited for simulating flow in the viscous sub-layer which has significantly influence on the accuracy of the results.

The governing equations for the SST k-ω model are [1]:

Turbulence Kinetic Energy

$$k: \quad \frac{\partial k}{\partial t} + U_j \frac{\partial k}{\partial x_j} = P_k - \beta^* k\omega + \frac{\partial}{\partial x_j}\left[(\nu + \sigma_k \nu_T)\frac{\partial k}{\partial x_j}\right] \qquad A-1$$

(I) (II) (III) (IV) (V)

Specific Dissipation Rate

$$\omega: \frac{\partial \omega}{\partial t} + U_j \frac{\partial \omega}{\partial x_j} = \frac{\alpha}{\nu_T} P_k - \beta \omega^2 + \frac{\partial}{\partial x_j}\left[(\nu + \sigma_\omega \nu_T)\frac{\partial \omega}{\partial x_j}\right] + 2(1 - F_1)\sigma_{\omega^2} \frac{1}{\omega}\frac{\partial k}{\partial x_i}\frac{\partial \omega}{\partial x_i} A-2$$

(I) (II) (III) (IV) (V) (VI)

The term (I)-(V) in equation A-1 and A-2 can be expressed as[2]:

Rate of change of k or ω

Transport of k or ω by convection

Rate of production of k or ω

Rate of dissipation of k or ω

Transport of k or ω by turbulent diffusion

The last term (VI) in equation A-2 is called the cross-diffusion term.

The kinematic eddy viscosity in this model is given by:

$$\nu_T = \frac{a_1 k}{max\ (a_1\omega, SF_2)} \qquad A-3$$

where S is the invariant measure of the strain rate, which is given by

$$S = \sqrt{2S_{ij}S_{ij}} \qquad A-4$$

$$S_{ij} = \frac{1}{2}\left(\frac{\partial U_i}{\partial x_j} + \frac{\partial U_j}{\partial x_i}\right) \qquad A-5$$

The first blending function is

$$F_1 = tanh\left\{\left\{\min\left[\max\left(\frac{\sqrt{k}}{\beta^*\omega y}, \frac{500\nu}{y^2\omega}\right), \frac{4\sigma_{\omega 2}k}{CD_{k\omega}y^2}\right]\right\}^4\right\} \qquad A-6$$

$$CD_{k\omega} = \max\left(2\rho\sigma_{\omega 2}\frac{1}{\omega}\frac{\partial k}{\partial x_i}\frac{\partial \omega}{\partial x_i}, 10^{-10}\right) \qquad A-7$$

The second blending function is

$$F_2 = tanh\left[\left[\max\left(\frac{2\sqrt{k}}{\beta^*\omega y}, \frac{500\nu}{y^2\omega}\right)\right]^2\right] \qquad A-8$$

where y is the distance to the nearest wall.

When the blending functions are equal to zero, the simulation region is away from the surface and a standard k-ε model is applied, while the blending functions are equal to one, the k-ω model is chosen to simulate the region that is inside the boundary layer.

The blending functions are not only raised to modify the cross-diffusion term in equation A-2, but also used for model constant, α.

$$\alpha = \alpha_1 F_1 + \alpha_2 (1 - F_1) \qquad A-9$$

It should be noted that a production limiter, P_k , prevents the build-up of turbulence in stagnation regions [3].

$$P_k = min\left(\tau_{ij}\frac{\partial U_i}{\partial x_j}, 10\beta^* k\omega\right) \qquad A-10$$

The SST k-ω model constants are as follows:

Table A.1 Constants for SST k-ω model

σ_{k1}=0.85	σ_{k2}=1.0	$\sigma_{\omega 1}$=0.5	$\sigma_{\omega 2}$=0.856	β_1=0.075
β_2=0.0828	β^*=0.09	a_1=0.31	α_1=5/9	α_2=0.44

References

[1] C. Rumsey, The Menter Shear Stress Transport Turbulence Model.Available at http://turbmodels.larc.nasa.gov/sst.html, 2013

[2] H.K. Versteeg, W. Malalasekera, An introduction to computational fluid dynamics: the finite volume method, Prentice Hall, 2007.

[3] F.R. Menter, Review of the shear-stress transport turbulence model experience from an industrial perspective, International Journal of Computational Fluid Dynamics, 23 (2009) 305-316.

APPENDIX B

Self-defined scalar transport solver

```
#  include "fvCFD.H"
#  include "IFstream.H"
#  include "OFstream.H"
#  include "simpleControl.H"

// * * * * * * * * * * * * * * * * * * * * * * * * * * * * * * * * * * * * * * * * * * * * //

int main(int argc, char *argv[])
{
#   include "setRootCase.H"
#   include "createTime.H"
#   include "createMesh.H"
#   include "createFields.H"

simpleControl simple(mesh);

// * * * * * * * * * * * * * * * * * * * * * * * * * * * * * * * * * * * * * * * * * * * * //

    Info<< "\nCalculating scalar transport\n" << endl;

#   include "CourantNo.H"

    ofstream output_file("Volfra.csv");

    while (simple.loop())
    {
       Info<< "Time = " << runTime.timeName() << nl << endl;

       while (simple.correctNonOrthogonal())
```

```
        {
         volScalarField DTEff = Dab+nut/ScTurb;

          solve
          (
              fvm::ddt(alpha1)
            + fvm::div(phi, alpha1)
            - fvm::laplacian(DTEff, alpha1)
          );
        }

        gradAlpha = fvc::grad(alpha1)/(1-alpha1.weightedAverage(mesh.V()).value());

        Info<< "Volume fraction = "
              << alpha1.weightedAverage(mesh.V()).value()
              << endl;

        output_file<< "Time = " << runTime.timeName() << ", "
                   << "Volume fraction = "
                   << alpha1.weightedAverage(mesh.V()).value()<<"\n"
                   << endl;

        runTime.write();
        Info<< "ExecutionTime = " << runTime.elapsedCpuTime() << " s"
            << "  ClockTime = " << runTime.elapsedClockTime() << " s"
            << nl << endl;
    }

    Info<< "End\n" << endl;

    return 0;
}

// ************************************************************************* //
```